

3-21-2017

Media Velocity Considerations in Pleated Air Filtration

Frederik Carl Schousboe

University of South Florida, fcschousboe@gmail.com

Follow this and additional works at: <http://scholarcommons.usf.edu/etd>

 Part of the [Mechanical Engineering Commons](#)

Scholar Commons Citation

Schousboe, Frederik Carl, "Media Velocity Considerations in Pleated Air Filtration" (2017). *Graduate Theses and Dissertations*.
<http://scholarcommons.usf.edu/etd/6632>

This Thesis is brought to you for free and open access by the Graduate School at Scholar Commons. It has been accepted for inclusion in Graduate Theses and Dissertations by an authorized administrator of Scholar Commons. For more information, please contact scholarcommons@usf.edu.

Media Velocity Considerations in Pleated Air Filtration

by

Frederik Carl Schousboe

A thesis submitted in partial fulfillment
of the requirements for the degree of
Master of Science in Mechanical Engineering
Department of Mechanical Engineering
College of Engineering
University of South Florida

Major Professor: Rasim Guldiken, Ph.D.
Nathan Crane, Ph.D.
Jose Porteiro, Ph.D.

Date of Approval:
March 10, 2017

Keywords: Pleatwise, Computational Fluid Dynamics, Maximum Media Velocity, Geometric Imperfection, Prediction

Copyright © 2017, Frederik Carl Schousboe

DEDICATION

I dedicate this work to Trése, Christian, and Owen Schousboe.

ACKNOWLEDGEMENTS

I would be remiss if I did not acknowledge the support and guidance I have received from Dr. Rasim Guldiken in the development of the ideas laid forth in the following pages, as well as his persistent positive influence, as an educator and mentor, upon me and my peers throughout my time at university. The direction and guidance of Dr. Jose Porteiro was likewise invaluable during my time as his student; his contributions to my academic and professional development have been profound. I would also like to thank Dr. Nathan Crane for his inputs as part of my outstanding thesis committee. Finally, I owe a debt of gratitude to the wonderful office staff in the mechanical engineering department at the University of South Florida.

TABLE OF CONTENTS

LIST OF TABLES	iii
LIST OF FIGURES	iv
ABSTRACT	v
CHAPTER 1: INTRODUCTION	1
1.1 Geometric Imperfections in Air Filtration	1
1.1.1 Geometric Imperfections at the Filter Scale	3
1.1.2 Geometric Imperfections at the Pleat Scale	4
1.2 Objectives	5
1.3 Thesis Organization	5
CHAPTER 2: BACKGROUND IN AIR FILTRATION	7
2.1 Significance of the Conditioned Environment	7
2.1.1 The Human Environment	7
2.1.2 The Industrial Environment	9
2.2 Key Performance Drivers in Air Filtration Applications	10
2.2.1 Separation Efficiency	11
2.2.2 Pressure Drop	12
2.3 Various Approaches to Air Filtration	13
2.3.1 Barrier Filtration	13
2.3.1.1 Surface Filtration	14
2.3.1.2 Depth Filtration	14
2.3.1.2.1 Inertial Impaction	15
2.3.1.2.2 Direct Interception	15
2.3.1.2.3 Diffusion	16
2.3.2 Inertial Separation	16
2.3.2.1 Vortex Tube Separators	18
2.3.3 Additional Filtration Approaches	19
2.3.3.1 Chemical Adsorption	19
2.3.3.2 Catalysts	19
CHAPTER 3: MODELS OF FLOW THROUGH A POROUS MEDIUM	21
3.1 Introduction to the Mathematical Flow Field	21
3.2 The Porous Zone	22
3.2.1 Darcy's Law	22
3.2.2 Brinkman's Modification	23
3.2.3 Lapwood's Modification	24

3.3 Application of the Mathematical Model	24
CHAPTER 4: SIMULATION MODEL FOR CURRENT WORK	27
4.1 Study Variables	27
4.1.1 Configuration Geometries	27
4.1.2 Investigated Velocities	29
4.2 Mesh Considerations	30
4.2.1 Mesh Type and Sizing	30
4.2.2 Mesh Statistics	31
4.3 Boundary and Cell Conditions	32
4.4 Solver Set-Up	33
4.5 Model Validation	34
4.5.1 Pressure Driven Flow between Fixed Parallel Plates	36
4.5.1.1 Analytical Solution	36
4.5.1.2 Simulation	37
4.5.2 Flow through a Porous Medium	38
CHAPTER 5: RESULTS AND DISCUSSION	40
5.1 Results Overview	40
5.2 Overall Velocity Profiles	42
5.3 Media Velocity Investigation	44
5.3.1 Media Velocity Profiles	44
5.3.2 Media Velocity Maximum Values	46
5.4 Relationship between Various Study Parameters	47
5.4.1 Dimensionless Comparisons	48
5.5 Evaluation of Maximum Media Velocities	50
5.5.1 Predictive Tools for Maximum Media Velocity	51
5.5.2 Correction Factor Tool	52
5.5.3 Linear Fitting Tool	53
CHAPTER 6: CONCLUSIONS AND FUTURE WORK	56
6.1 Conclusions	56
6.2 Future Work	58
LIST OF REFERENCES	59
APPENDIX A: COMPLETE SIMULATION RESULTS	61
APPENDIX B: LYDAIR 4450HS PRODUCT DATASHEET	65
APPENDIX C: COPYRIGHT PERMISSIONS	68

LIST OF TABLES

Table 2.1 Adapted MERV Rating Table from ASHRAE Standard 52.2	8
Table 2.2 Overview of Standard Rating Schemes for High Performance Air Filters	10
Table 4.1 Various Parameters of a Single Simulation Configuration	30
Table 5.1 Overview of Simulation Results	41
Table 5.2 Absolute Relative Percent Error, Uniform Flow Assumption	51
Table 5.3 Absolute Relative Percent Error, Correction Factor Tool	53
Table 5.4 Investigation of Slope Fitting Parameter, Linear Fitting Tool	54
Table 5.5 Investigation of Y-Intercept Fitting Parameter, Linear Fitting Tool	54
Table 5.6 Absolute Relative Percent Error, Linear Fitting Tool	55

LIST OF FIGURES

Figure 1.1 Pleated filter scales	1
Figure 1.2 Filter scale velocity profiles	3
Figure 1.3 Pleat scale velocity profiles	4
Figure 3.1 Typical regions for mathematical pleat considerations	21
Figure 4.1 Typical pleat geometry for current study	28
Figure 4.2 Simulation boundary and cell conditions	32
Figure 4.3 Plot of typical scaled residuals	34
Figure 4.4 Overview of two systems used for model validation	35
Figure 5.1 Representative pleatwise media velocity distribution	40
Figure 5.2 Overall velocity profiles for various cases	42
Figure 5.3 Media velocity profiles for various cases	45
Figure 5.4 Example of probe tool being used to evaluate local filtration velocity	47
Figure 5.5 Plot of V_{max}/V_{avg} vs. aspect ratio	48
Figure 5.6 Plot of V_{max}^2/V_{avg}^2 vs. aspect ratio	49
Figure 5.7 Plot of V_{max} vs. V_{avg} for various pleat configurations	50

ABSTRACT

Asset protection in the form of fluid filtration makes up an ever-increasing part of the civilized and industrialized world. Fluid filtration applications in the conditioned environment and life sciences are affording the world's population a chance to better realize their potential, while industrial applications help ensure that high demand processes can be carried out safely, reliably, and effectively.

In the present work, a tool has been developed, using the computational fluid dynamics package FLUENT, to allow the designer to better predict the magnitude of geometric imperfections within a given pleat configuration.

Pleated rectangular filters, intended to improve the quality of air for human occupants, with a U-shaped pleat form have been chosen as the focus of this study. A simulation study is developed to investigate the maximum local velocity normal to the filtration surface and to characterize the magnitude of the pleatwise velocity distribution across a range of pleated geometries and flow conditions. The geometry of the U-shaped pleat form can be characterized by, amongst other parameters, the width of the pleat channel, the overall height of the individual pleat, as well as the thickness of the filtration medium. The various geometries of the current study were developed by changing the width of the pleat channel, as well as the channel height, while keeping the medium thickness constant throughout. Changing the width of the pleat channel allows the designer to achieve varying pleat densities, expressed as a number of pleats along a one inch section of the overall pleated pack. Pleat densities of 6.5, 7, 7.5, 8, and 8.5 pleats per inch are considered in the current study. Pleat heights of 1.0, 0.75, and 0.50 inches are

also investigated in the current study. Furthermore, the filter velocity can be characterized by the free stream velocity at the face of the filter pack, termed the face velocity, and by the velocity of the fluid at the interface with the filtration medium, referred to as media velocity. In the present work, the face velocity was adjusted in each case to achieve the desired media velocities across the study, which are 10.5, 9.0, 7.5, and 6.0 feet per minute.

In an effort to more clearly communicate the results of the study, the results are presented in the form of a non-dimensionalized plots which present the designer with a way to quickly gauge the effect of pleat geometry on maximum velocity. Additionally, two tools are presented to aid the designer in more accurately predicting the maximum filtration velocity. These tools are then evaluated for effectiveness using the method of absolute relative percent error. The assumption of uniform flow through the filtration media leads to an average absolute relative percent error of 27%. The first tool the reader is presented with is a simple correction factor which predicts the maximum filtration velocity with an average absolute relative percent error of 10% over the study domain. The second tool, which takes a slightly more complicated y-intercept form, characterizes the maximum filtration velocity as a function of average velocity and aspect ratio. This approach further reduces the average absolute relative percent error to 4%.

The results of the simulation herein are successfully employed to develop a set of simple yet effective tools that allow the filter designer to more accurately predict maximum velocities through a pleated air filter.

CHAPTER 1: INTRODUCTION

1.1 Geometric Imperfections in Air Filtration

In many applications, a chosen filtration medium is constructed in a pleated configuration to better maximize the available filtration area and reduce the system losses. One particular application which employs this technique extensively for both human occupants and industrial components is air filtration [1]. There are multitudes of commercially available filtration media that have been designed, tested, and marketed for countless types of air filtration applications.

When considering pleated air filters, it is helpful to have a concept of various scales to better understand the interactions between the fluid and the filter, as well as filtration medium [2] [3]. Figure 1.1, below, provides a context for the discussion of scales. The first scale presented is what is referred to as the filter scale; this scale allows the designer to understand the air flow in the duct leading to and leaving the pleated filter. The second scale presented in this thesis is the pleat scale; this scale allows the designer to understand the interaction at the fluid/filtration media interface.

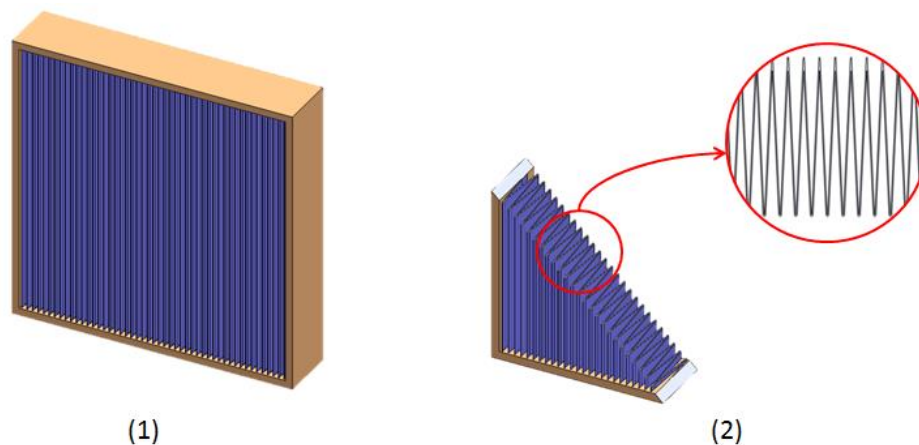


Figure 1.1 Pleated filter scales. (1) The full filter scale and (2) the pleat scale.

Performance of the filtration media is often the most significant contributor to filter performance. Many commercial manufacturers go to great lengths to define the specific performance characteristics of the various grades available to the filter designer, these characterizations are almost always carried out on flat sheet samples; leaving the filter designer with the task of evaluating and optimizing his/her filter design against the applicable application requirements. This task is complicated due to the geometric imperfections that arise in the flow field. Recently, the proliferation of access to reliable computational fluid dynamics tools has led to new opportunities in fields dedicated to studying functional performance characteristics of pleated air filters. The contributions to this effort from academia have been invaluable. Many papers have been published regarding pleat form optimization for clean pressure drop [4] [5] [3] as well as instantaneous pressure drop modeling as the pleated filtration medium builds up a dust cake [6] [7]. Another area of concern for the filter design is initial separation efficiency. Separation efficiency, or penetration, is also a parameter that is often specified by the commercial manufacturer of the filtration medium in the flat sheet condition, where the media is challenged with a uniform flow at a known velocity. However, the pleated configuration of many air filters causes the fluid flow to deviate from uniformity; this deviation away from uniformity can be thought of as a geometric imperfection imposed by the very nature of the pleated filter pack, and exists in addition to the non-uniform flow through the duct. Quantifying the extent of the geometric imperfections is a difficult task to accomplish analytically and many filters are unnecessarily over designed, despite the availability of the types of tools mentioned above, while others are made to go through extensive redesign efforts in order to achieve acceptable levels of particulate separation efficiency.

1.1.1 Geometric Imperfections at the Filter Scale

Considering the full filter scale, imperfections arise from the very nature of flow through a duct, as shown in the image below. While it is convenient to evaluate a filter against a uniform flow assumption, by dividing the flow rate by the face area of the filter, using Equation 1 below, this has the potential to start the entire design process off on the wrong foot.

$$U_{mean} = \frac{Q}{A} \quad (1)$$

where U_{mean} is the magnitude of an assumed uniform flow distribution along the length of section, Q is the total volumetric flow rate, and A is the cross-sectional area of the duct.

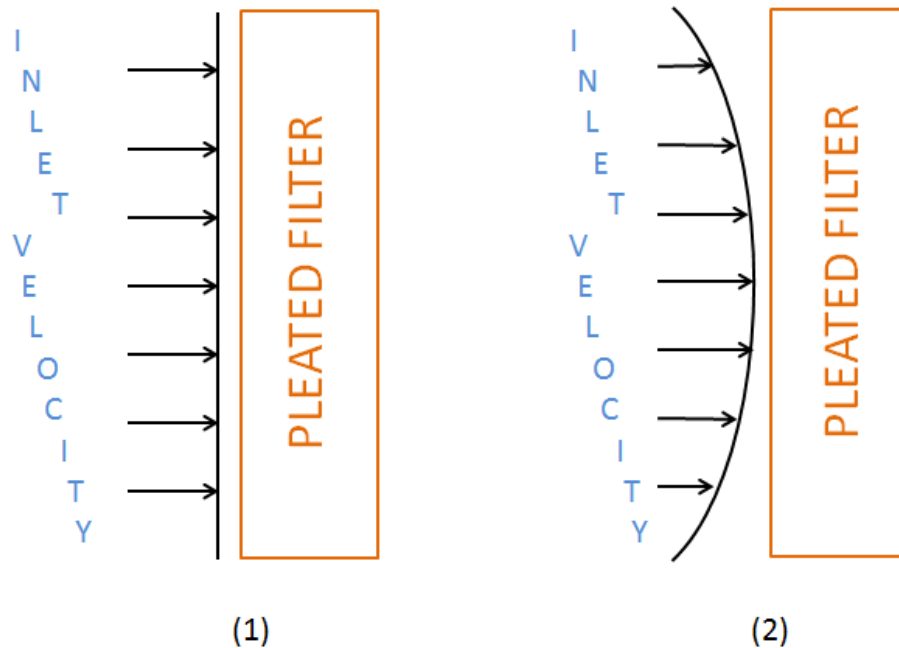


Figure 1.2 Filter scale velocity profiles. (1) Uniform flow distribution and (2) non-uniform flow distribution.

Another approach may be to evaluate the flow in the duct to determine the maximum inlet velocity using any one of a number of formulations or with the aid of rudimentary computational fluid dynamics modeling. For example, the maximum velocity for a pressure driven flow between two parallel plates can be derived from the mean velocity by evaluating the following expression

$$U_{max} = \frac{3}{2} U_{mean} \quad (2)$$

where U_{max} is the maximum component of velocity along the length of section and U_{mean} is the average velocity in the same direction. Figure 1.2, above, provides the reader with an illustration of this concept. The field of study related to velocity distribution in various ducts has been well studied and is beyond the scope of the present work. A thorough review of such work can be found in reference [8].

1.1.2 Geometric Imperfections at the Pleat Scale

Similar to the full filter scale, when considering the pleat scale there is also a non-uniform velocity distribution along the flank of the pleat. Figure 1.3 below is an exaggeration intended to give the reader a conceptual understanding of what a theoretical velocity distribution may look like. It is the intent of the present work to develop a simulation which characterizes the distribution of filtration velocity along the length of the pleat and employ the results of the simulation in an effort to build a simple model that will allow the designer to better predict the magnitude of the maximum filtration velocity early in the design phase.

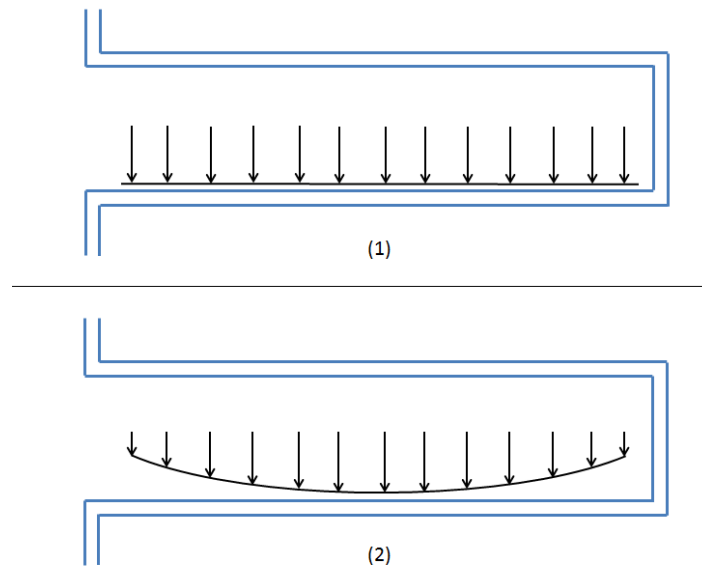


Figure 1.3 Pleat scale velocity profiles. Uniform flow distribution (1) and non-uniform flow distribution (2).

1.2 Objectives

The objectives for the current work can be captured in the bullet points below:

- Develop a model to simulate flow through a pleated air filter using the readily available computational fluids dynamics solver FLUENT built into ANSYS Workbench.
- Investigate the effects of pleat geometry on the magnitude of geometric imperfections in the pleat scale, due to the geometric imperfections in flow distribution.
- Present a non-dimensional relationship between the aspect ratio of a U-shaped pleat and the maximum media velocity, normalized to the theoretical average media velocity that follows from the uniform flow assumption.
- Develop a toolset to allow the filter designer to better predict the maximum filtration velocity.

1.3 Thesis Organization

The following thesis is presented such that Chapter 2 provides the reader with an overview of air filtration fundamentals, and defines many of the terms employed throughout. The chapter details are listed below to aid the reader in developing a better conceptual overview of present work.

- Chapter 2 introduces a few of the many applications of air filtrations, followed by an overview of various approaches to air filtration. The reader is then presented with many of the key performance drivers for typical air filtration applications.
- Chapter 3 puts forth a discussion concerning the development of many of the underlying mathematical models used to evaluate pleated air filters.
- Chapter 4 details the study variables, modeling approach, and a substantiation of the model employed in the current study.

- Chapter 5 presents the results from the current study followed by a discussion of their significance.
- Chapter 6 discusses the conclusions from the current work and considerations for future work.

CHAPTER 2: BACKGROUND IN AIR FILTRATION

2.1 Significance of the Conditioned Environment

As the human race has advanced and developed into a more sophisticated and productive species so too has the need for air filtration. Which has grown increasingly complex and efficient as new applications and performance demands are driven by the course of human development [1] [9]. The applications for air filtration, while diverse and ever expanding, can be thought of in two main categories: enhancements to the occupied conditioned environment and asset protection for industrial processes. While there is undoubtedly some overlap between the two, and niche examples that do not lend themselves to either, the following employs these two categories as an appropriate means to introduce the reader to air filtration.

2.1.1 The Human Environment

Consideration of the conditioned environment for human occupancy, nowadays referred to as Indoor Air Quality (IAQ), is believed to have begun in earnest in the 1960s with the publication of studies from Scandinavia exploring issues related to thermal comfort [10]. Shortly thereafter, the American Society of Heating, Refrigeration and Air-Conditioning Engineers (ASHRAE) began to develop and maintain a set of standards aimed at helping design and characterize building systems with the indoor conditioned environment in mind. ASHRAE Standard 55, *Thermal Environmental Conditions for Human Occupancy*, was first published in 1966 and is intended to define the combination of factors that lead to generally acceptable indoor environments [11]. Another ASHRAE standard, aimed at defining and measuring requirements related to ventilation for IAQ, was first published in 1973 [12]. It wasn't until 1992, however,

that the first ASHRAE standard related to the characterization of air filtration was put forth. Standard 52.1 was published with the stated purpose to “establish test procedures for evaluating the performance of air-cleaning devices for removing particulate matter” [13]. A need for thorough laboratory data was understood and after several years of testing and discussions a follow-on specification was published, ASHRAE 52.2 [14]. This work has since superseded the original specification and now serves as the standard for characterizing the performance of many air filtration products designed for the human occupied environment. Standard 52.2 defines a method for characterizing filters by not only investigating their ability to arrest particles in the clean condition, but as the filter is loaded with a synthetic dust to simulate real world loading as well. The final reported value from this testing is referred to as the minimum efficiency reporting value, or MERV, of the filter. Table 2-1 is adapted from the ASHRAE standard and is intended to provide the reader context regarding the parameters of common air filtration testing. Note that the filtration rating is not independent of the size of the contamination challenge.

Table 2.1 Adapted MERV Rating Table from ASHRAE Standard 52.2 [14]

Standard 52.2 Minimum Efficiency Reporting Value (MERV)	Composite Average Particle Size Efficiency, % in Size Range, μm		
	Range 1 0.30 - 1.0	Range 2 1.0 - 3.0	Range 3 3.0 - 10.0
1	n/a	n/a	$E_3 < 20$
2	n/a	n/a	$E_3 < 20$
3	n/a	n/a	$E_3 < 20$
4	n/a	n/a	$E_3 < 20$
5	n/a	n/a	$20 \leq E_2 < 35$
6	n/a	n/a	$35 \leq E_2 < 50$
7	n/a	n/a	$50 \leq E_2 < 70$
8	n/a	n/a	$70 \leq E_2$
9	n/a	$E_2 < 50$	$85 \leq E_2$
10	n/a	$50 \leq E_2 < 65$	$85 \leq E_2$
11	n/a	$65 \leq E_2 < 80$	$85 \leq E_2$
12	n/a	$80 \leq E_2$	$90 \leq E_2$
13	$E_1 < 75$	$90 \leq E_2$	$90 \leq E_2$
14	$75 \leq E_1 < 85$	$90 \leq E_2$	$90 \leq E_2$
15	$85 \leq E_1 < 95$	$90 \leq E_2$	$90 \leq E_2$
16	$95 \leq E_1$	$95 \leq E_2$	$95 \leq E_2$

While the multitudes of ASHRAE standards are aimed at the conditioned environments in buildings, both residential and commercial/industrial; the rise of air travel has led to concerns over the quality of air in the occupied spaces of commercial passenger aircraft. Cabin air quality is covered by the following specification: SAE AIR 4476.

2.1.2 The Industrial Environment

The need for air filtration in the industrial environment grew alongside the developments related to IAQ discussed in the previous section. Just as the first studies and standards regarding the conditioned environment were coming into existence the need for higher levels of protection for many industrial applications was also being realized. One example of this was the development, in 1969, of an improved inlet protection method for two-wheel motor vehicles by a team of entrepreneurs who owned and operated a motorcycle sales and maintenance outlet, which included a factory race team [15]. A study from the same time period, commissioned by the US Army and executed by the International Harvester company identified the cost associated with the overhaul and maintenance of erosion damaged helicopter turbines in South East Asia as about 150 million dollars per year [16]. More recently, the growth in semi-conductor manufacturing has necessitated new advances in the field of air filtration. Semi-conductor chips are made in an environment where filtration levels limit airborne contaminant to less than one dust particle per cubic foot and exchange the air in the clean room on the order of 10 times every minute [17]. The higher levels of particulate filtration required by today's processes push, and in many cases, exceed the levels defined by the MERV scale, detailed previously. As a result, there are many additional specifications in existence in order to provide acceptable means of compliance for higher performing air filtration products. The proliferation of various standards has caused confusion in industry and efforts are underway to align and centralize many of the

current standards. Table 2-2 gives an overview of two the current standards, in addition to ASHRAE 52.2, that are in place for characterizing air filter performance.

Table 2.2 Overview of Standard Rating Schemes for High Performance Air Filters

<u>IEST-RP-CC001</u>		<u>BS - EN 1822</u>	
Rating	Minimum % Efficiency	Rating	Minimum % Efficiency
HEPA (Type A)	99.97 per MIL-STD-282	E10	≥ 85
HEPA (Type C)	99.99 per MIL-STD-282	E11	≥ 95
HEPA (Type D)	99.999 per MIL-STD-282	E12	≥ 99.5
ULPA (Type F)	99.9995 @ 0.1-0.2 or 0.2-0.3 μm	H13	≥ 99.95
Super ULPA (Type G)	99.9999 @ 0.1-0.2 or 0.2-0.3 μm	H14	≥ 99.995
HEPA (Type H)	99.97 @ 0.1-0.2 or 0.2-0.3 μm	U15	≥ 99.9995
HEPA (Type J)	99.99 @ 0.1-0.2 or 0.2-0.3 μm	U16	≥ 99.99995
HEPA (Type K)	99.995 @ 0.1-0.2 or 0.2-0.3 μm	U17	≥ 99.999995

2.2 Key Performance Drivers in Air Filtration Applications

As was previously mentioned, air filtration is, at its heart, a means to accomplish asset protection. Whether it be the human respiratory system or a complex manufacturing operation, ensuring that people and process perform at their best is what air filtration is all about. It is only

natural then to begin a discussion of the history of air filtration with an introduction to various ways in which effectiveness is measured, however air filters are typically one part of a much larger system. In addition to separation efficiency, air filters are typically categorized by their initial added resistance when placed within a system, and the amount of loading they can withstand before placing too large of a load on the rest of the system.

2.2.1 Separation Efficiency

Perhaps the most important performance parameter of any pleated air filter (the kind of air filter considered in this thesis), is its effectiveness when challenged with a representative contaminant [7]. There have been many ways in which the effectiveness of air filters has been characterized (see section 2.1 for an overview of such). Effectiveness of a particular filter is driven largely by two main factors; the velocity of the fluid to be filtered as it moves through the filter, and the size range of the airborne particulate to be filtered [18]. Figure 2, of the above referenced standard BS EN 1822-1, illustrates both of these factors. It can be seen that the data corresponding to the lower filtration velocity produces higher efficiency results. What may be a little more difficult to discern is the effect of particle size on filtration velocity. Both data sets in the referenced image, the 1.5 cm/sec velocity as well as the 3.0 cm/sec velocity, illustrate that there is a minimum efficiency as a function of particle size. This is because particles in this size range are more likely to follow the streamlines of the air passing through the filter and as such will avoid contact with the filtration medium. Particles any larger than this will have too much inertia to be pulled by the shear viscous forces exerted by the air, while particles any smaller than this will follow Brownian motion and be captured through diffusion mechanisms [1]. The actual particle size which forms the minimum may differ between applications, however whichever particle size is the minimum for each application is referred to as the Most Penetrating Particle

Size or MPPS [18]. For a deeper review of particle capture mechanisms in depth filtration medium, see section 2.3.1.2. The dependence of effectiveness on velocity and particle size is further illustrated by the manufacture's product datasheet, included herein as Appendix B. The dependence of separation efficiency on fluid velocity is the driving force behind the current work, as it has proven to be difficult to accurately predict the fluid velocity at the fluid filtration interface.

2.2.2 Pressure Drop

In addition to the effectiveness of the filter at arresting the unwanted contaminate, the amount of work required to push or draw the air through the filter is another important parameter. The magnitude of the pressure loss through the filter is typically specified as single pressure loss value that denotes the change in pressure from just upstream of the filter to just downstream of the filter. Pressure loss is commonly measured in Pascals, Pounds per Square Inch, and Inches of Water Column. When the pressure loss is measured in pounds per square inch the units are denoted as "psid" to denote the frame of reference. Pressure loss across the filter has a large impact on the larger system as a whole as this will drive fan/source selection and as well as drive power considerations [7]. Minimizing the clean pressure drop through an air filter was the goal of many of the early works which sought to characterize flow through a filter using computational fluid dynamics [4, 5]. These papers found that by balancing the viscous and inertial losses of flow through a pleated medium the overall pressure loss through a clean filter could be minimized. Pressure loss, however, is not a fixed parameter for all filtration applications. While some systems continually expel the contaminant from the system, such as those found in Section 2.3.2, leading to a relative constant pressure loss over time, barrier systems that employ pleated filtration media will experience a temporal change in pressure loss

as contaminant builds up on the filtration surface [2, 19]. Recent work in the field of filter simulation using computational fluid dynamics has been carried out to help the designer predict the loading dependent changes in pressure.

2.3 Various Approaches to Air Filtration

In the realm of air filtration, the specific developments are most likely too numerous to list in their entirety. Below the reader is presented with an overview of three various approaches to air filtration, with an emphasis on what is referred to as barrier filtration as this encompasses the type of filtration solution studied in this thesis.

2.3.1 Barrier Filtration

Perhaps the most basic type of barrier filtration can be thought of as a net, whose behavior is quite simple to understand. However, the concept of providing a physical barrier through which a fluid passes with the intention of removing some undesirable constituent of that fluid can, and indeed does, become much more involved than a simple net. A filtration system that employs a single layer net like structure is often referred to as surface filtration, because the unwanted particles are caught in the net and build upon its surface. However, it is possible to layer fibers on top of one another, not in the form of a net, to increase many of the performance parameters of the simple net filter. This type of filtration solution is referred to as depth filtration. In either form barrier filters, can be tailored, via materials selection and design, to achieve almost any filtration rating. Barrier filters themselves are mostly simple devices; they typically interact in a passive fashion with the larger system and require minimal system modification. The performance of barrier filters changes as a function of loading, where the pressure differential across the filter increases as more and more contaminant is captured by the filter.

2.3.1.1 Surface Filtration

To say that surface type filters represent a simple case of filtration is somewhat of a misnomer, in that many of the manufacturing techniques associated with today's surface filters are anything but simple. Take for instance the TEMISH NTF9000 line of filtration products from Nitto Denko. This product line is an example of a surface type of filtration medium, where precise pores are created in a membrane and are sized to prohibit the passing of particles over a certain size rating. However, the manufacturing techniques used to produce the material are anything but simple.

The predominant capture mechanism for surface filters can be thought of as an advanced sieving mechanism, as surface filters capture any particle that is too large to pass through the pore structure. For these types of filters, the effectiveness of the medium will not change if a second layer is added in series as the capture mechanism of the surface filter is simply the size of the pore in the filter medium; this is why they are referred to as surface filters [1].

The collection of particles on the surface of a filter can carry with it a number of benefits. Chief among them are the ability to wash and reuse the filter as well as the potential to collect the contaminant that is arrested [20]. However, as contaminant is loaded onto the surface of the filtration medium the pressure loss through the filter system increases much more rapidly with surface filters as opposed to depth filtration media, this forms one of the largest limitations of surface filtration.

2.3.1.2 Depth Filtration

Depth filtration is different from surface filtration in that the mechanisms of capture are not as straight forward as for surface filters and the performance characteristics of depth filters changes differently as a function of time when compared to surface filtration. The mechanisms

of particle capture for depth filtration media are: Inertial Impaction, Direct Interception, and Diffusion. It is important to note that while all three mechanisms can be addressed separately, all three will act simultaneously in real world applications. All three mechanisms can be thought to work together to contribute to a total single fiber efficiency for a given depth filtration medium. The following presents a cursory review of the mechanics of depth filtration, however much work has been done to address the topic in detail and the reader is referred to references [1] [21] for further information.

2.3.1.2.1 Inertial Impaction

As air flows through a depth filtration medium it must change direction to flow around the fibers in its path. When a particle's inertia is high enough that the drag exerted on it by the airflow is not sufficient to alter the particles trajectory and the particle makes contact with the fiber, this is referred to as inertial impaction. It is important to note that the particle's size and density play a large role in this mechanism of capture, as does the Stokes drag exerted on the particle by the fluid. The equation used to characterize separation by inertial impaction is referred to as the Stokes number and is defined as:

$$St = \frac{d_p^2 \rho U}{18 \mu d_f} \quad (3)$$

where d_p is the particle diameter, ρ is the density of the particle, U is the free stream velocity of the fluid, μ is the dynamic viscosity of the fluid, and d_f is the fiber diameter [1]. Particles having a higher stokes number are less likely to follow the streamline of the fluid and thus have a higher chance of impacting a fiber due to their inertia.

2.3.1.2.2 Direct Interception

There can still be an interception of those particles which follow the streamline of the fluid flow through a depth filtration medium, despite the particle not being arrested via inertial

impaction. Direct interception is the term used to describe when a particle following the streamline of the fluid comes in direct contact with a fiber in the depth filtration medium. If the particle follows a path that is less than one particle radius away from the fiber, then it is assumed that it will adhere to the fiber and be captured.

It should be noted that a particle may be intercepted by a combination of inertial impaction and direct interception. In the case of a particle flowing through the medium with a low Stokes number that does not necessarily follow the streamline of the fluid in which it was originally traveling, the particle can in theory deviate from the stream line and still “miss” the fiber; likewise, a particle may deviate from its original path and still strike the fiber.

2.3.1.2.3 Diffusion

As particle diameter continues to decrease neither of the two aforementioned capture mechanisms dominate the separation of particles from the fluid stream. Particles in this size range quickly reach thermal equilibrium with the gas that surrounds them; resulting in the particles undergoing what is referred to as Brownian motion [1]. In this condition the average velocity of the smaller particles will be greater than that of larger particles. Under Brownian motion, the capture of a particle by what is termed diffusional deposition is a function of the magnitude of the diffusional motion and the convective motion of the fluid around the fiber.

2.3.2 Inertial Separation

Another approach to air filtration is to split an incoming air stream into two paths where one path requires an abrupt change in geometry that the particles are unable to follow. These types of systems are referred to as inertial particle separators (IPS) and have been used to protect the turbo-machinery of turbo shaft powered helicopters for quite some time [22]. There are two main types of inertial particle separators: a forward facing IPS as well as an axially integrated

IPS. These may be used independently or in conjunction with one another. The reader is directed to US Patent 4,389,227 for a conceptual overview of the front facing IPS [23]. For a conceptual overview of the axial IPS the reader is directed to US Patent 3,832,086 [24].

In the case of the front facing IPS the incoming air stream is accelerated outward in a duct whose cross section is simultaneously reduced while its inner diameter is increased. This serves to impart inertia on the particles as they move through the section. The flow is then dissected, some of the flow follows the inner contours of the ducting and is directed into the engine while the flow at the outer portion of the duct, and the heavier particles, are ejected overboard [25]. The axial style IPS, unlike the front facing version, is typically designed by the engine manufacturer and is more integrated into the rotorcraft engine [25]

A filtration system using inertial separator has two key advantages. The first comes from the somewhat steady state behavior of the separation system. Unlike barrier filtration solutions the contaminate challenge is thoroughly expelled from the system all together, as opposed to being collected within the system. This, as well as a distinct lack of moving parts, means that not only do inertial separators maintain their performance throughout their lifetime they also require very little maintenance.

There are, however, some limitations to these systems. For one, the limit of their separation effectiveness, while high, is typically understood to be less than that of what can be achieved using various porous media (barrier filtration). Also, in most applications the flow that is used to scavenge the particle laden air requires a source to be driven. This can add substantial cost and/or complexity to the initial system design and procurement.

2.3.2.1 Vortex Tube Separators

Vortex tube separators are a subset of the larger family of filtration devices referred to as inertial separators which act to remove particulates from a supply air stream by passing the incoming air through some change in geometry. Vortex tube separators accomplish this by employing what is referred to as a vortex generator, hence the name. In this arrangement, an inlet tube contains a vortex generator which imparts a swirl to the flow as it passes into the inlet tube, because the flow now has a tangential and radial component of velocity in addition to the incoming axial velocity, and causes the heavier (compared to air) particles to move to the extremes of the tube. The shape of the vanes that make up the vortex generator also cause the particles to move outward due to the incident angle of the incoming particle upon impact with the vane. A concentric tube of a smaller diameter is located downstream of the vortex generator, after some length in the axial direction to allow the particles to move to the outer portions of the larger tube, and directs the “filtered” air in the core of the tube to the end point of use, while the outer particulate laden portion of the flow is scavenged and discarded [26]. For a conceptual view of typical vortex tube arrangement the reader is directed to US Patent 7,879,123 [27].

Vortex tube separators have been used as single inline tube style filters as well as an array of multiple tubes to protect the intakes of rotorcraft as well as land based heavy equipment. One application that lends itself to the single tube inertial separator is filtering hot bleed air from a jet engine. Because of the very nature of its operation the single tube vortex separator has no moving parts and can be fabricated from materials that can withstand the intense heat and elevated temperatures of engine bleed air. When used as intake protection for rotorcraft applications the tubes are employed as an array that can be formed into a panel. Using multiple

tubes increases the available throughput of the inertial separation system and limits the pressure losses through the array.

2.3.3 Additional Filtration Approaches

The two filtration approaches identified thus far have focused on the removal of dust or dirt particles from a given working fluid, however dirt and dust are not the only unwanted contaminants found in air systems. Among the multitudes of non-dust or dirt contaminants are Volatile Organic Compounds (VOCs) and ozone. Both of these contaminants can also be filtered out of an air supply using the two techniques covered below.

2.3.3.1 Chemical Adsorption

A common approach to removing Volatile Organic Compounds is to employ what is referred to as a chemical adsorption filter. Many chemical adsorbers act very much like a barrier filtration medium; however, in this instance undesired chemicals are adsorbed onto a solid surface that is tuned to attract the unwanted chemical constituent. Chemical adsorbers tend to decrease in efficiency as they load with contaminant, thus many are designed to be disposable [28]. In air filtration applications, it is not uncommon to see these types of adsorbers installed in series with a pleated barrier filtration media, which are also many times a disposable item.

2.3.3.2 Catalysts

Ozone, while not present in high levels at sea level, can reach much higher concentration levels at higher altitudes [29]. This poses a problem to aircraft operating at such altitudes, as ozone can damage some of the onboard systems. For this reason there have been many applications of ozone catalyst on commercial aircraft operating at high altitudes [28]. A typical ozone catalyst works to oxidize the O_3 molecule as it passes through the filter giving off three molecules of O_2 for every two molecules of O_3 that enter the system. The structure often consists

of a honeycomb substrate material coated with any one of a number of known chemical compounds, such as manganese dioxide, platinum or palladium depending on the exact application and the presence of additional contaminants. Catalysts, unlike chemical adsorbers, require heat to carry out the chemical reaction and as such are most commonly found in the hot section of the pneumatic supply air when found on aerospace applications [28].

CHAPTER 3: MODELS OF FLOW THROUGH A POROUS MEDIUM

3.1 Introduction to the Mathematical Flow Field

When considering the flow through a pleated medium, it is helpful to separate the problem into various regions. A common approach to this is presented in Figure 3.1, where a single pleat of a filter is presented. In the figure, the upstream channel and downstream channel represent areas of free fluid flow and the media region represents the chosen filtration medium. As air flows through this pleat arrangement, there are several sources of pressure losses [4]. The first being contraction losses as the flow is directed into the pleat channel. As the flow moves along the pleat channel, both upstream and downstream, there are viscous forces acting between the fluid and the filtration media, this leads to the second source of losses. As the fluid passes through the filtration medium, there exists a third loss due to interaction in the porous zone. Finally, as the fluid leaves the pleated configuration, the flow will experience expansion losses.

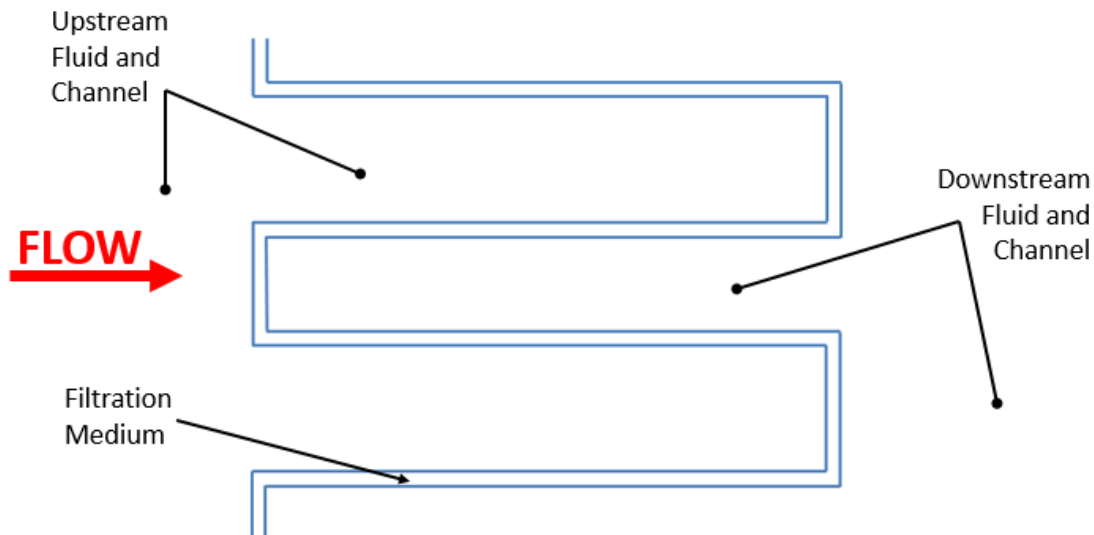


Figure 3.1 Typical regions for mathematical pleat considerations.

The flow in the upstream and downstream channels is governed by the Navier-Stokes momentum and continuity equations [5]. In employing these models, it is helpful to apply the following assumptions: the flow is steady, is incompressible, is composed of an isotropic homogenous fluid, and that the velocity profile at the far upstream of the flow field is uniform.

Consideration of the flow through the filtration medium has been the subject of work for some period of time. Kuwabara was able to adapt the Stokes flow equation to describe the forces acting upon parallel cylinders under the Stokes flow condition, by considering the filter make up as a lattice of cylinders [30]. The cell model developed by Kuwabara is used extensively to better understand the interactions between particles and fibers at the fiber scale, however this approach does not work well at the filter or pleat scale. The approach that has been employed in recent developments, with great success, is to model the filtration medium as a porous zone using Darcy's equation.

3.2 The Porous Zone

Pressure driven flow through a porous medium is an important phenomenon with relevant applications far beyond the evaluation of flow through filtration media [31]. Darcy's law is often used to relate the velocity of a fluid through a porous zone. Applications outside the field of air filtration include: ground water hydrology, petroleum engineering, agricultural engineering, and soil mechanics [32].

3.2.1 Darcy's Law

In its most basic form Darcy's equation defines the pressure loss through a porous zone as:

$$\nabla p = -\frac{\mu}{k} \vec{v} \quad (4)$$

where Δp is the pressure loss, μ is the fluid viscosity, k is a constant of proportionality intrinsic to the porous medium, and \vec{v} is the fluid velocity [5]. Modeling the flow through the porous zone using Darcy's equation has several limitations [4]; the flow is assumed to be homogeneous, there is no account for interactions at the interface between the fluid and the porous medium, the results only hold true where flow rates are relatively small, and in the case of low pressure gasses the presence of slip flow cause the system to deviate from Darcy's law. The first and fourth limitations do not apply to most studies of air filtration and much work has been done to remedy the remaining two.

3.2.2 Brinkman's Modification

The limitation of Darcy's law at the fluid medium interface arises from the evaluation of the condition of Stokes flow in the fluid flow field. The governing equation for Stokes flow is given by:

$$\nabla p = \mu \nabla^2 \vec{v} \quad (5)$$

where ∇p is the pressure gradient, μ is the fluid viscosity, and \vec{v} is the fluid velocity [31]. It can be seen that the Stokes flow equation includes a second order velocity term whereas the equation used to describe Darcy's flow does not. This inevitably leads to issues when evaluating boundary conditions for various applications and considerations must be made. This has historically been done by adding a body dampening term to Darcy's equation which distinguishes between the viscosity of the fluid and an apparent viscosity of the fluid in the porous medium. This modification to Darcy's equation is often referred to as Brinkman's term which is the second term on the right-hand side of the equation:

$$\nabla p = -\frac{\mu}{k} \vec{v} + \mu_e \nabla^2 \vec{v} \quad (6)$$

where μ_e is a fitting term used to define the viscosity of the fluid in the porous zone [31]. Here the value of k goes to infinity in the free stream fluid and one is left with the definition of Stokes flow.

3.2.3 Lapwood's Modification

Drawing from its widespread application outside of fluid filtration, the limitation of low velocity flows was alleviated by the addition of a convective term. Developed to study the transfer of heat through porous media, a term referred to as the Lapwood modification was added to the Darcy equation yielding the Darcy-Lapwood-Brinkman (DLB) equation:

$$\nabla p = -\frac{\mu}{k} \vec{v} - \frac{\rho}{\varepsilon^2} \nabla \vec{v} + \mu_e \nabla^2 \vec{v} \quad (7)$$

where ε is the porosity of the media [5]. This now allows for the study of flows at higher velocities.

3.3 Application of the Mathematical Model

Darcy's law and the many permutations of it have been applied in a variety of disciplines as noted previously. In the realm of air filtration, the solutions were applied first to develop semi-analytical solutions and then progressed into the development of full finite element models.

In 1992, Yu and Goulding developed a semi-analytical solution to solve for pressure drop across pleated filter packs [33]. Their work was aimed at providing increased levels of protection for ground based gas powered electricity generation turbines using aerospace derived turbine technologies. The model solved the flow field in the upstream and downstream channels using the Navier-Stokes equations for motion. Then a constant suction/injection model was developed and applied to the boundaries at the interface of the media. The flow through the porous media was solved for by employing the simple form of Darcy's law based on the permeability of the media. The media channels along the pleats were discretized and solution was developed by

evaluating the upstream, media, and downstream conditions simultaneously. The Yu/Goulding model was later refined by Chen et al in 1995. The refinement included integrating the solution into a full finite element model by discretizing the upstream and downstream fluid zones as well as the media section, and employing the Darcy-Lapwood-Brinkman model to more accurately predict the performance of the pleated pack [4].

The work by Yu/Goulding as well as Chen et al, gave the designer a very useful tool to understand the effects of various parameters on clean pressure drop performance. Both studies developed models that predicted an optimal pleat count configuration for clean filter design. Optimum pleat count is the number of pleats for a certain height that will minimize the combined pressure loss due to the drop through the filtration media as well as the viscous forces along the flank of the pleat. Less pleats would lead to the velocity of the air moving through the media needing additional driving force in the form of a larger pressure differential, while any more pleats will increase the surface area of media that the flow is forced to travel along as it moves down the pleat.

More recently, work has been done to understand the effects of dust cake formation on a filters pressure loss performance [6] [7] [19]. In these works, the contaminant particles are introduced into the study and agglomerated onto the surface of the filtration medium. However, the filtration media used in most applications where substantial dust collection is expected are typically depth filtration media. Thus, models that consider the collection of particles to be on the surface tend to not properly capture the effects of dust loading. Also, once a dust cake begins to form its permeability is not constant, as more dust loads the pressure drop across the media and dust cake increases leading to compaction of the dust cake and changes in its permeability. There have been studies aimed at understanding the formation of a dust cake and the way its

permeability changes as a function of time [34]. However, none of these models consider the tendency of the individual pleat to deform under loading; when this takes place, pleat channels are closed off and the flow changes dramatically in the neighboring pleats.

In the current thesis, the commercially available FLUENT CFD solver is employed to model the air flow through a single pleat, drawing from the work of Chen et al, and the component of velocity normal to the pleat is investigated. This is done to provide the designer with a tool to better evaluate the initial efficiency of a pleated filter, as efficiency is strongly tied to the media velocity.

CHAPTER 4: SIMULATION MODEL FOR CURRENT WORK

Building upon the work of the previous authors, a computational fluid dynamics study was carried out to gain a more thorough conceptual understanding of the flow field through a pleated air filtration medium [4, 5]. The study was conducted using the commercially available FLUENT solver included in ANSYS Workbench 15.0. LydAir MG 4450HS, a typical commercially available air medium used to achieve HEPA level filtration ratings, was used throughout the study. The product datasheet, including specifics concerning the media, can be found in Appendix B.

4.1 Study Variables

The current thesis examines an array of various pleat configurations and velocities in order to investigate the relationship between the maximum pleatwise filtration velocity and the design reference point of average media velocity. The geometries and flow rates are detailed below.

4.1.1 Configuration Geometries

The current study considers several geometries of the U-shaped pleat configuration, because they are representative of current manufacturing technologies. The study considers three pleat heights, 0.5 inches, 0.75 inches, and 1.0 inch. The width of the pleat was varied as well to achieve various aspect ratios at each pleat height. The parameter of pleat width is seldom used in the design and manufacture of pleated filter packs, however, and it is more common to characterize the pleat width by referring to the pleat density or the number of pleats per inch. That is to say that if the pleated filter pack has an overall length of ten inches and the designer

has specified a total of 100 pleats, the pleat density would simply be 10 pleats per inch. This would yield a pleat width of 0.100 inches. It is important to note that the pleat width varies from the channel gap, for the U-shaped pleat, by a factor of 2 to 1. For the pleat width specified above, the pleat gap would be 0.050 inches. The pleat densities chosen for the current studies are: 6.0, 6.5, 7.0, 7.5, 8.0 and 8.5. The general shape of the pleat can be described by the non-dimensional ratio of pleat width to pleat height defined by the equation below:

$$AR = \frac{w}{h} \quad (8)$$

where AR is the aspect ratio, w is the pleat width, and h is the pleat height. Figure 4.1, below, gives an overview of the typical pleat arrangement as modeled in the current work, the overall pleat channel width of 0.133” corresponds to a pleat density of 7.5 pleats per inch.

For the purposes of the current work, edge effects were neglected and symmetry was assumed applicable to the bounds of the single pleat configuration. This approach was observed throughout the current literature review and has been shown to yield reasonable results for pressure drop [2, 4, 5].

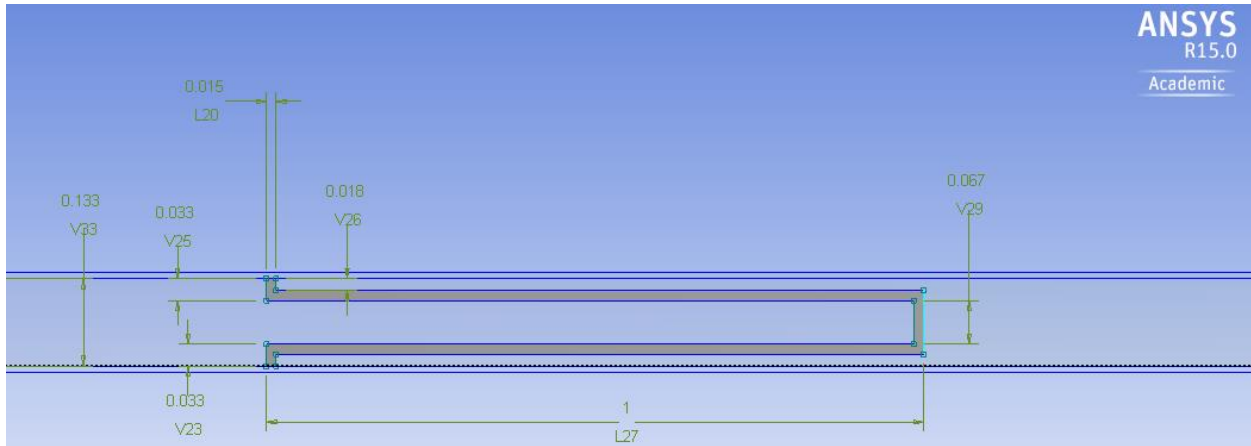


Figure 4.1 Typical pleat geometry for current study.

4.1.2 Investigated Velocities

Furthermore, the study also investigated several filtration media velocities. Beginning with the media velocity at which the material is rated, 10.5 ft/min, and incrementing to values of 9.0, 7.5, and 6.0 ft/min. To achieve the desired average media velocity, a pack having the overall dimensions of 10" x 10" x 1" was evaluated for each geometry and a free stream face velocity was prescribed for each flow rate that would yield the desired media velocity. It was assumed that the duct in which the filter was installed was of a constant cross sectional area equal to that of the filter face. Edge effects and boundary layers were neglected for the purposes of this study. The filter media area of the pleated pack was determined using the following equation:

$$A = 2 \times PH \times PL \times W \quad (9)$$

where A is the total media area, PH is the pleat height, PL is the number of pleats in the pack, and W is the overall pack width. By evaluating the total media area, the desired media velocity, and the cross-sectional area of the duct, a free stream face velocity was assigned for all cases. Table 4-1 below gives the reader a detailed overview of the various parameters for the single configuration with a pleat density of 6.5 pleats per inch and a media velocity of 10.5 ft/min. The general approach throughout the study was to multiply the total media area in units of square feet, by the desired filtration media velocity in feet per minute. The resulting volumetric flow rate having units of cubic feet per minute was then divided by the cross-sectional area of the duct, expressed in square feet, to determine the free stream linear velocity for the particular case. The Reynolds number in the duct was also calculated for each case and can be found in Appendix A.

Table 4.1 Various Parameters of Single Simulation Configuration

Parameter	Value	Units
Face Area	100	in^2
Slit Width	10	in^2
Length of Pack	10	in^2
Pleat Height	1	in^2
Mean Media Velocity (Vavg)	10.5	ft/min
Media Thickness	0.015	in
PPI	6.5	$1/in$
Pleat Width	0.15385	in
Aspect Ratio	0.15385	
Number of Pleats	65	#
Media Area	9.02778	ft^2
Volumetric Flow Rate	94.7917	$ACFM$
Face Velocity	136.5	ft/min

4.2 Mesh Considerations

As with any simulation, there are certain considerations that must be made of the manner in which the system is discretized, or meshed. The number of nodes and elements, the quality of the mesh, the skewness of the mesh, and the mesh aspect ratio are all commonly investigated to typify the overall suitability of the discretization of the simulated regime [35]. The mesh statistics for the 7.5 pleat per inch and 1" pleat height configuration are discussed in detail herein; the reader is directed to Appendix A for referencing the other configurations.

4.2.1 Mesh Type and Sizing

The mesh for the current study was created while leveraging as many of the default settings as possible. The settings related to physics and solver preferences were left unchanged with the values of CFD and Fluent respectively. One best practice for mesh sizing from industry is to ensure that there is a minimum of three elements across the thinnest section of any system to be discretized. With this in mind, it was determined that the mesh for the current simulation should be controlled with an element size of 0.005 inches as the filtration medium is 0.015 inches thick, and the mesh was updated with a face sizing command with a specified element

size of 0.005 inches. Due to the simple two-dimensional nature of the system this mesh size was prescribed throughout the simulation domain. The mesh for the configuration referenced above consisted of 22,265 nodes and 21,447 elements.

4.2.2 Mesh Statistics

As mentioned previously, there are several methods available to help the analyst objectively evaluate the discretization of their system. A few common metrics are; Element Quality, Aspect ratio, and Skewness [35].

Evaluation of element quality is a method that allows the analyst to characterize the volume of the element as a ratio to the sum of the square of the element edge lengths. A value of 1 denotes a perfect square element while values closer to zero indicate issues related to the volume of the element. For this study, the discretization scheme was found to have an average element quality of 0.994, with a standard deviation of .0197.

Aspect ratio is a way to quantify how far from square a particular element may be. For reference, a square would have an aspect ratio of one and a long slender rectangle would have an aspect ratio much larger than one. A general rule of thumb is to limit the maximum aspect ratio to be between 3 and 5, although there may be some instances where this is not practical. Higher aspect ratios can be a source for errors especially in simulations that investigate stress and displacement as very long slender elements may not follow the small deflection assumption present in many linear finite element analyses. The mesh scheme for the 7.5 PPI 1 inch pleat height element had a maximum aspect ratio value of 1.828, an average of 1.033, and a standard deviation of 0.0367.

Skewness is yet another measure commonly employed to help understand the appropriateness of a given discretization scheme. Skewness is viewed as one of the foundational

metrics for mesh evaluation, it evaluates how close to equilateral (or equiangular for non-triangular meshes) the cell structure is thorough out the simulation domain. A square, or equiangular element, would be given assigned a value of 0 while a highly-skewed element would be assigned a value approaching one. Values of skewness less than 0.25 are termed “good” and it is suggested that for two-dimensional studies a quality grid will have an average skewness of 0.1 and that all elements within a quality two-dimensional mesh should be “good or better” [35]. In the current study the mesh is found to have a typical skewness of 0.001 and a max element skewness of 0.23.

As all of the metrics for mesh suitability indicate that the discretization scheme for the current work is in-line with acceptable limits, the mesh size was considered adequate and the study was carried out with the rule of thumb of three elements across any constituent of the domain.

4.3 Boundary and Cell Conditions

Several boundary conditions were assigned in the simulation to represent the actual system. Figure 4.2 below provides a system overview. As discussed previously, symmetry was applied to the upper and lower bounding surfaces.

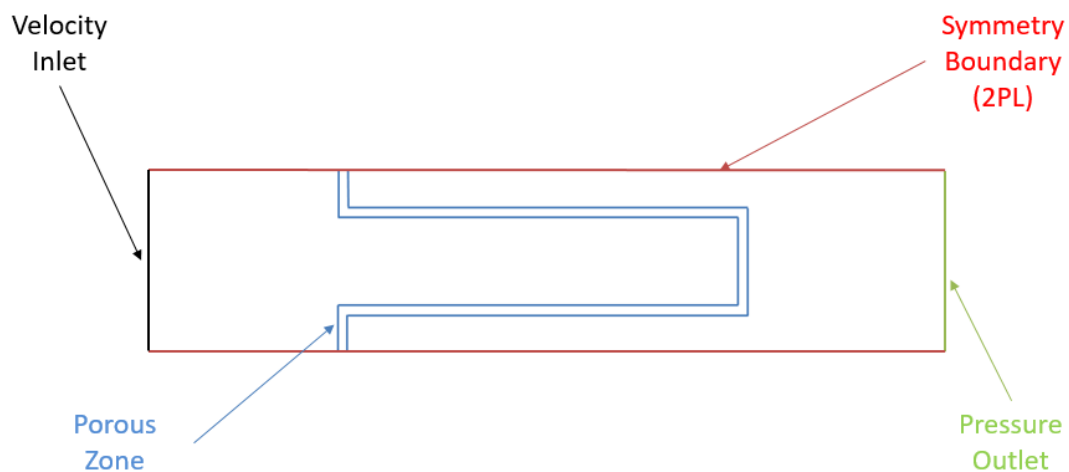


Figure 4.2 Simulation boundary and cell conditions.

The system was modeled using a prescribed velocity boundary condition at the inlet and a pressure boundary at the outlet. The inlet velocity was adjusted for each configuration to correspond with the free stream face velocity. The pressure was held constant at zero pressure (gauge pressure not absolute) throughout all configurations of the study. The filtration media was simulated using a porous cell, or porous zone, within the FLUENT domain. The porous zone was initially assigned a viscous resistance term using the procedures for such detailed in the ANSYS user's guide. This was adjusted to match the flat sheet data provided in the filtration media supplier datasheet, provided for reference in Appendix B. The resistance value for the filtration media for the current study was determined to be $8.126 \times 10^{11} \text{ m}^{-2}$. Based on observations from the industry, the permeability in the tip and trough of the pleat was reduced by a factor of 10^3 , to account for damage during manufacturing [36].

4.4 Solver Set-Up

The system was evaluated using the FLUENT solver integrated in ANSYS Workbench 15.0, the following will describe the solution controls that were updated by the user to perform the current study.

The Fluent solver was initialized with the 2-D and Double Precision options selected. The solver settings were chosen to be as follows:

- Type – Pressure Based
- Velocity Formulation – Absolute
- Time – Steady
- 2-D Space – Planar

The simulation was solved using the Viscous- Laminar model, as the Reynolds number for all configurations was well below 2000. The solution Methods were assigned as the following:

- Scheme – SIMPLE
- Gradient – Least Squared Cell Based
- Pressure – Second Order
- Momentum – Second Order Upwind

The default under relaxation factors of 0.3, 1, 1, and 0.7 were maintained for pressure, density, body forces, and momentum, respectively. The simulations were run for 300 iterations each, and the scaled residuals of continuity, x-velocity, and y-velocity were monitored for convergence throughout. Figure 4.3 below gives an example of the residuals plot for the 7.5 pleats per inch, one inch pleat height, 10.5 ft/min filtration velocity configuration.

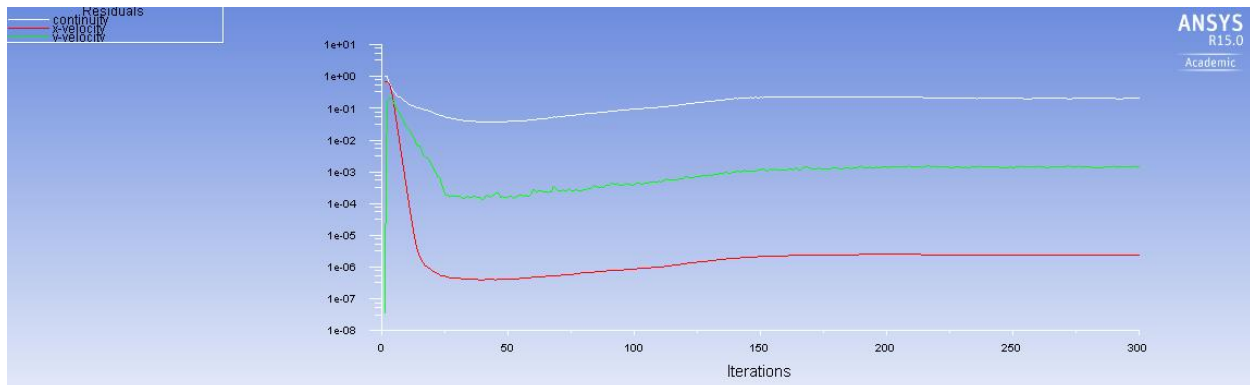


Figure 4.3 Plot of typical scaled residuals.

4.5 Model Validation

As part of building a robust model and becoming familiar with the FLUENT interface, two systems for which a relatively straight forward solution exists were modeled and investigated; a simple case of pressure-driven flow between two fixed parallel plates and flow through a flat sheet of porous medium with known parameters. Figure 4.4 below gives an

overview of both systems. The maximum velocity and pressure loss through each system were investigated to ensure the model was producing reasonable results.

In both cases, the scale of the system was chosen to be representative of the final model. The width of the channel was prescribed as 0.133 inches, which is equivalent to a pleat density of 7.5 plats per inch. The system conditions were also chosen to represent the final model. A mean velocity of 10.5 ft/min was prescribed at the inlet, and a gauge pressure of zero was assigned at the outlet. A commercial available grade of air filtration media was chosen for the porous zone with a published pressure loss of 4.12×10^{-2} psi at a media velocity of 10.5 ft/min.

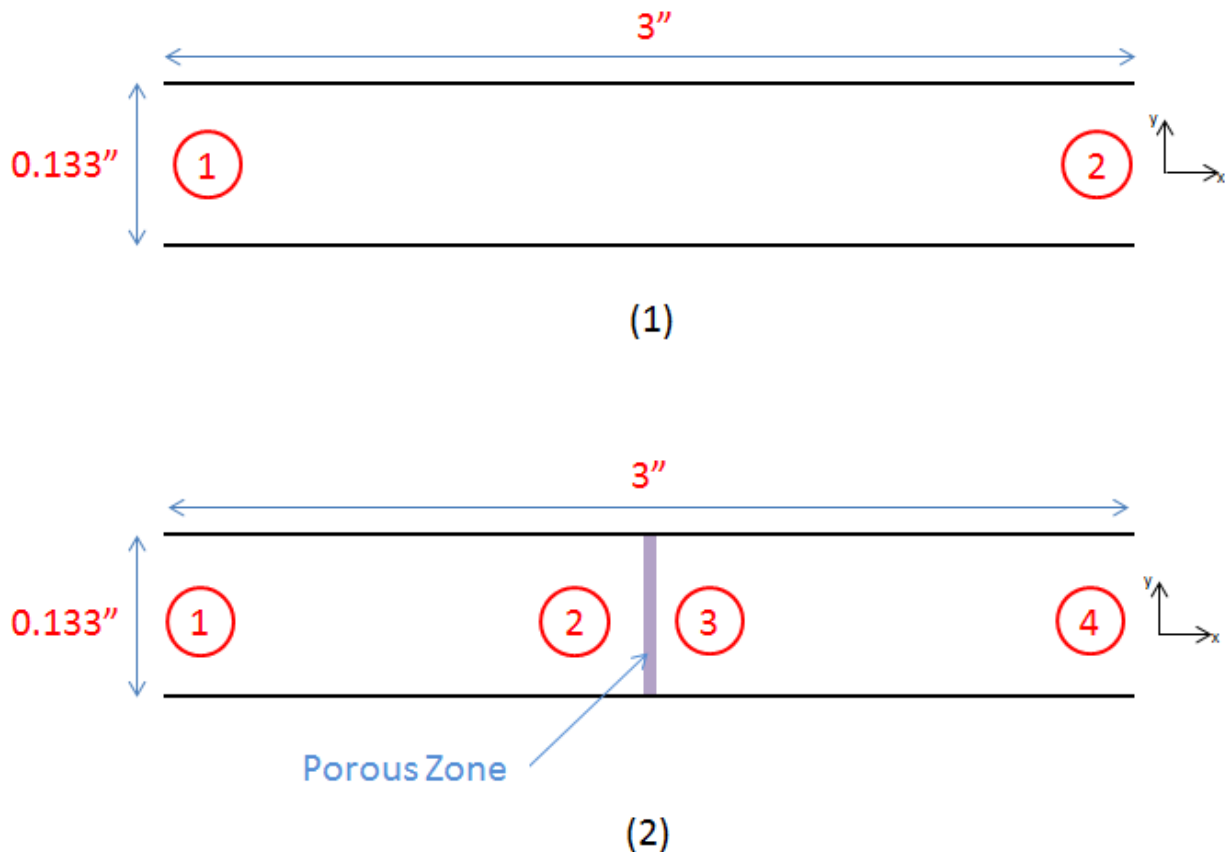


Figure 4.4 Overview of two systems used for model validation. Diagram of pressure driven flow between fixed parallel plates (1) and flow through a flat sheet filter medium (2).

4.5.1 Pressure Driven Flow between Fixed Parallel Plates

4.5.1.1 Analytical Solution

The first step in the analytical solution is to investigate the flow regime of the fluid in the system prescribed previously. This step will be carried out using the Reynolds number. The Reynolds number is defined by the following:

$$Re = \frac{\rho V D}{\mu} \quad (10)$$

where ρ is the density of the fluid, V is the fluid velocity, D is the characteristic diameter of the flow channel, and μ is the dynamic viscosity of the fluid [37]. Taking the fluid density as 2.28×10^{-3} slugs/ft³, the velocity as 0.175 ft/s, applying the channel width of 0.133 inches as the characteristic diameter, and the dynamic viscosity as 3.74×10^{-7} lb s/ft² yields a value of 11.84 for the Reynolds number. Defining the laminar flow regime as having a Reynolds number less than 2000, the flow is shown to be laminar.

To ensure that the fluid flow was fully developed the channel length was chosen to be at least 2 times the minimum entrance and exit length. The entry length, Le , for laminar flow is determined using the following equation:

$$Le = D \times 0.06Re \quad (11)$$

where D is the characteristic channel diameter (expressed in meters) and Re is the Reynolds number [37]. Taking the channel width to be the characteristic diameter and using the Reynolds number from above the minimum entry length is determined to be 0.94 inches. Thus, the overall channel length was chosen to be 3 inches. Furthermore, the plates were assumed to extend infinitely in the direction orthogonal to the xy -plane; the effects of gravity were also neglected.

To determine the maximum velocity the following equation was evaluated:

$$U_{max} = \frac{3}{2} U_{mean} \quad (12)$$

where U_{max} is the maximum velocity and U_{mean} is the average velocity [37]. Substituting the value of 10.5 ft/min yields a maximum velocity of 15.75 ft/min

To evaluate the pressure loss through the system the following equation was evaluated:

$$U_{mean} = \frac{h^2 \Delta P}{3\mu l} \quad (13)$$

where U_{mean} is the average velocity, h is half of the channel height, μ is the dynamic viscosity of air, ΔP is the change in pressure, and l is the channel length [37]. Rearranging to solve for the pressure loss per unit length yields

$$\frac{\Delta P}{l} = \frac{U_{mean} 3\mu}{h^2} \quad (14)$$

4.5.1.2 Simulation

The simulation was carried out using the FLUENT module for ANSYS Workbench 2015. The case was simulated using a two-dimensional approach with the flow field modeled by a simple rectangle. The dimensions were the same as those from the previous section. The model space was discretized using 0.0133" elements, with a total of 2,260 elements and 2,497 nodes. The upper and lower bounds of the flow field were prescribed as wall boundaries. The inlet was assigned as a velocity inlet with a mean velocity of 10.5 ft/min. The outlet was initialized as a pressure boundary, with a gauge pressure of zero.

By the 26th iteration the scaled residual of continuity as well as x and y velocity were deemed to have converged and the simulation was halted. The simulation returned a result for the max velocity of 14.70 ft/min representing a relative error of 6.7%. The simulation returned a result for pressure loss of 1.1×10^{-5} psi representing a relative error of 17%.

4.5.2 Flow through a Porous Medium

For the purposes of this investigation, a readily available commercial media with published performance characteristics was chosen to allow us to make comparisons between the model and the published datasheet. The datasheet is attached herein as an Appendix B.

The simulation was carried out using the FLUENT module included in ANSYS Workbench 2015. The flow field was modeled using a series of three rectangles, chosen to represent the fluid region upstream of the porous zone, the porous zone itself, and finally the fluid downstream from the porous zone. The dimensions were the same as the previous section with the addition of the porous zone which was modeled as having a thickness of 0.0145” based off of the supplier datasheet. The model space was discretized using 0.005” elements, with a total of 16,281 elements and 16,912 nodes. The upper and lower bounds of the flow field were prescribed as wall boundaries. The inlet was assigned as a velocity inlet with a mean velocity of 10 ft/min. The outlet was initialized as a pressure boundary, with a gauge pressure of zero. The porous zone was assigned a permeability of 4.101×10^9 1/m² using the steps outlined in the FLUENT user’s guide section titled “Deriving the Porous Coefficients Based on Experimental Pressure and Velocity Data”. The inertial loss through the media was neglected as the flow through the channels is laminar and the viscous losses dominate this region [36].

After the 35th solution step the simulation was deemed to have converged and the simulation was stopped. As with the previous study, the max velocity returned by the simulation was in the middle of the channel. The value was 14.70 ft/min, yielding the same relative error as before of 6.7%. The simulation returned a pressure loss across the porous medium of 2.25×10^{-4} psi. With a real value of 4.12×10^{-2} from the supplier datasheet this yields a relative error of 99.5%.

Upon further review, it was determined that the viscous losses through the media should follow Darcy's law, and indeed the FLUENT User Guide references this equation in its explanation. As the Darcy equation describes a simple linear relationship, it was inferred that the pressure loss error could be corrected by scaling the permeability factor in the software to achieve the desired results. This time the simulation reached a state of convergence after only 32 steps. The magnitude of the free stream velocity remained unchanged with a max velocity matching that of the previous studies, 14.7 ft/min. The pressure loss through the medium in this instance was 4.14×10^{-2} psi. This results in a relative error of 0.6%.

The model accurately predicted the velocity through both systems as well as the pressure drop through the first study. Furthermore, by scaling the permeability factor for the porous zone we were able to replicate the results presented by the manufacturer for velocity through the porous zone. It should be noted that the width of the channel in the exercise may cause the required entry and exit length for fully developed flow to deviate from the length determined using Equation 11, and that this is one possible source for the 6.7% error in the maximum velocity. Nonetheless, these results were determined to indicate that the model is suitable for the proposed study.

CHAPTER 5: RESULTS AND DISCUSSION

5.1 Results Overview

The simulation discussed in Chapter 4 was used to evaluate an array of various pleat configurations and average media velocities. The results allowed for the investigation of the overall velocity profiles, the absolute media velocities, and the relationship between the simulated maximum media velocity, average media velocity, and pleat configuration.

In general, the results from the simulations agreed with estimations. A distribution of media velocity was demonstrated along the length of the pleat, however, unlike the projected distribution, see Figure 1.2(1), the velocity spiked close to the pleat inlet and remained somewhat constant along the remaining length of the pleat. See Figure 5.1 for further reference.

Furthermore, a single non-dimensional relationship between aspect ratio and maximum velocity normalized to average velocity was sought. While this turned out not to be the case, a useful tool is developed and demonstrated nonetheless in Section 5.4.

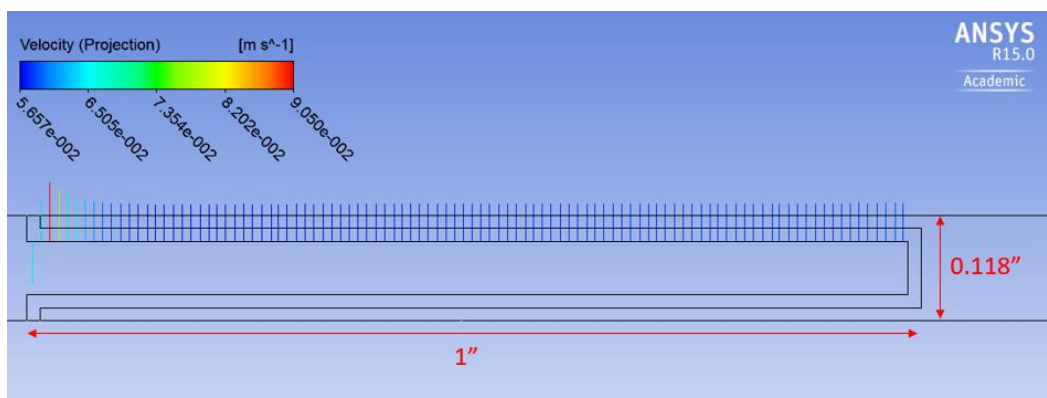


Figure 5.1 Representative pleatwise media velocity distribution.

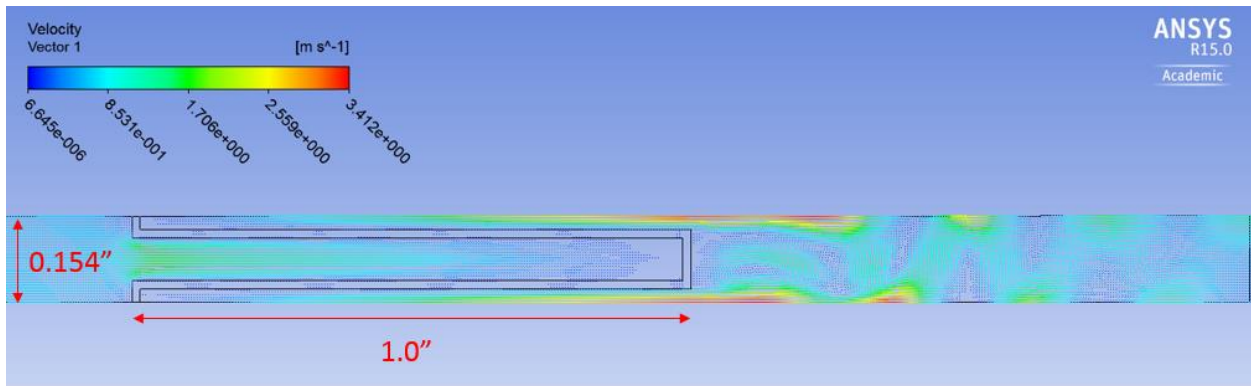
Table 5.1 below, gives the reader an overview of the simulation results. For a detailed listing of the results with the corresponding geometry parameters the reader is directed to Appendix A.

Table 5.1 Overview of Simulation Results

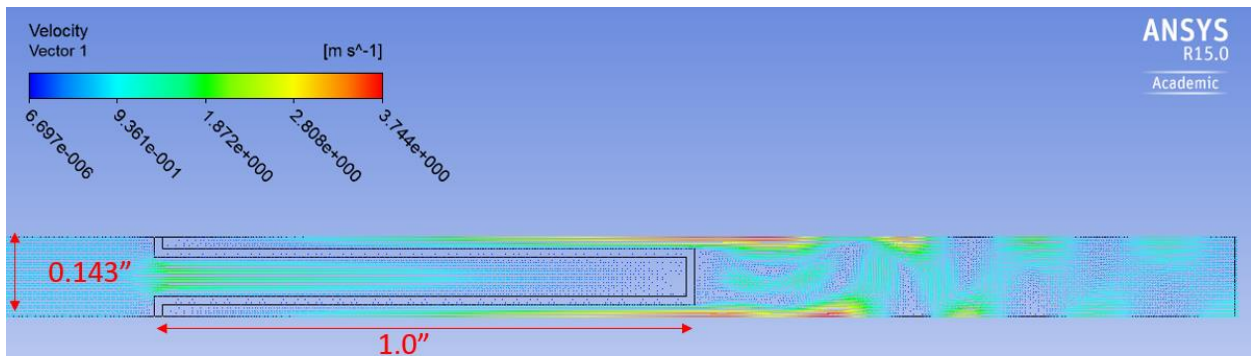
Simulation Results				
Pleat Density (pleats per inch)	Pleat Height (inches)	Average Media Velocity (ft/min)	Max Media Velocity (ft/min)	Pressure Drop (psid)
6.5	1.00	10.5	16.33	1.25
	1.00	9.0	13.18	1.07
	1.00	7.5	10.43	0.89
	1.00	6.0	7.68	0.71
	0.75	10.5	14.17	1.25
	0.75	7.5	9.25	0.89
	0.50	10.5	12.79	1.26
	0.50	7.5	8.66	0.90
7.0	1.00	10.5	16.92	1.25
	1.00	9.0	13.58	1.07
	1.00	7.5	10.63	0.89
	1.00	6.0	7.87	0.71
	0.75	10.5	14.57	1.25
	0.75	7.5	9.45	0.90
	0.50	10.5	12.79	1.27
	0.50	7.5	8.66	0.90
7.5	1.00	10.5	17.32	1.26
	1.00	9.0	13.97	1.08
	1.00	7.5	10.83	0.90
	1.00	6.0	8.07	0.71
	0.75	10.5	14.76	1.26
	0.75	7.5	9.65	0.90
	0.50	10.5	12.99	1.27
	0.50	7.5	8.66	0.90
8.0	1.00	10.5	17.72	1.28
	1.00	9.0	13.97	1.09
	1.00	7.5	10.83	0.91
	1.00	6.0	8.07	0.72
	0.75	10.5	15.16	1.26
	0.75	7.5	9.65	0.90
	0.50	10.5	12.99	1.27
	0.50	7.5	8.86	0.91
8.5	1.00	10.5	18.11	1.30
	1.00	9.0	14.57	1.11
	1.00	7.5	11.22	0.92
	1.00	6.0	8.27	0.73
	0.75	10.5	15.35	1.28
	0.75	7.5	9.84	0.91
	0.50	10.5	13.19	1.28
	0.50	7.5	8.86	1.32

5.2 Overall Velocity Profiles

In order to judge the appropriateness of the current work, the overall velocity profiles were investigated. The velocity profile results for the current thesis align with previous work. From the vector plots shown in Figures 5.2a through 5.2e, the reader can clearly see the flow contraction zone as well as the expansion zone discussed previously as sources of pressure losses through pleated porous media. While the flow field in the downstream area appears to tend away from laminar as it undergoes expansion, the maximum calculated value for Reynolds number in the free stream flow field, 178, is well short of the value where transition to turbulent flow typically begins.

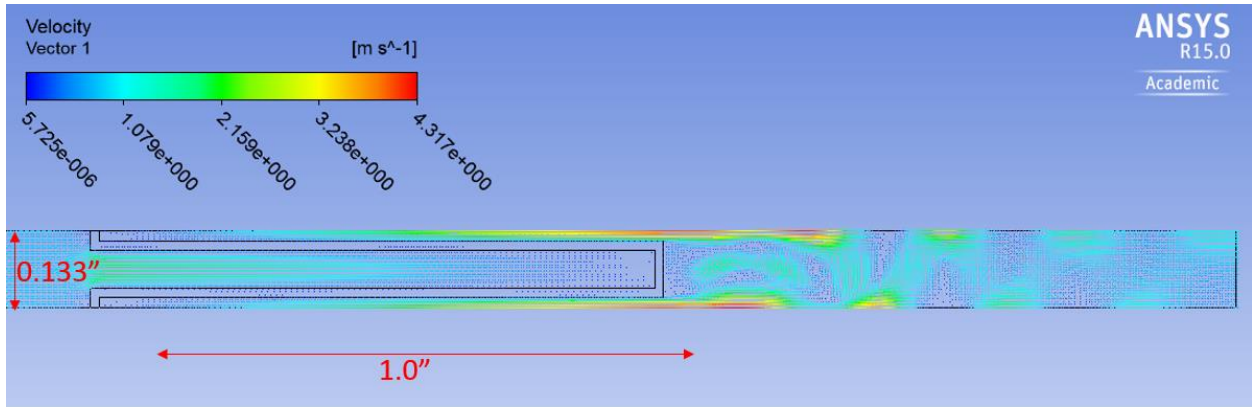


(a)

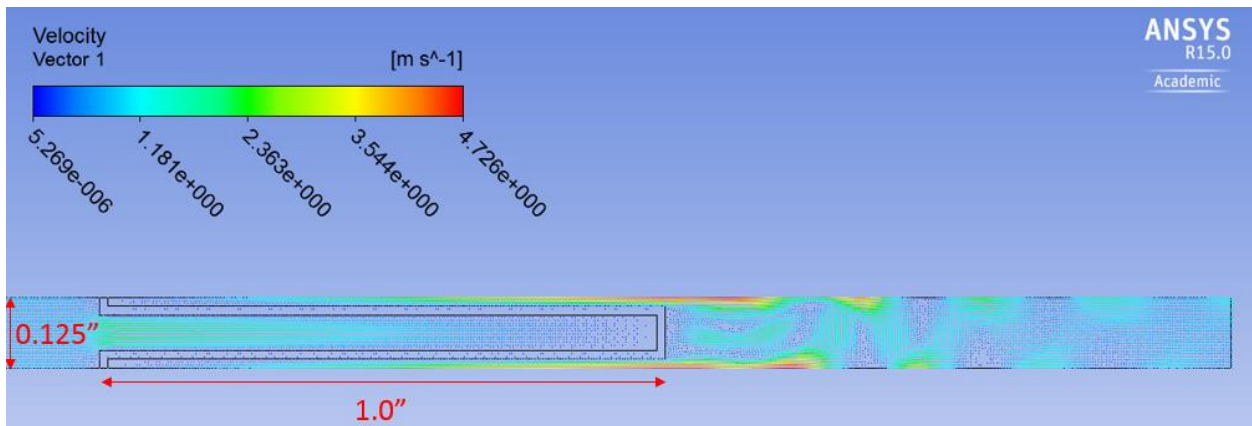


(b)

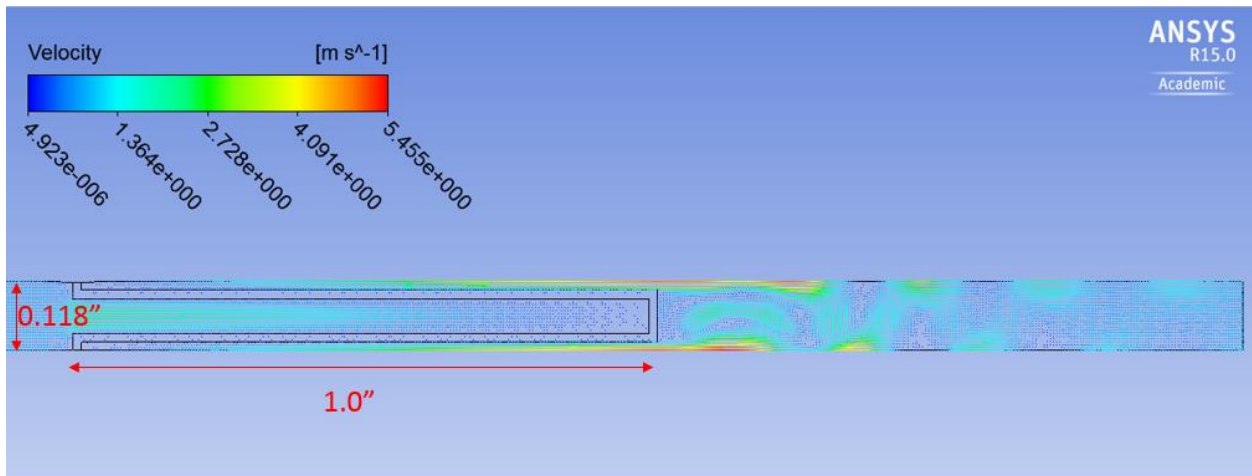
Figure 5.2 Overall velocity profiles for various cases. Each case having a 10.5 ft/min assumed uniform media velocity with pleat configurations 1 inch in pleat height and (a) 6.5 pleats per inch (b) 7.0 pleats per inch (c) 7.5 pleats per inch (d) 8.0 pleats per inch and (e) 8.5 pleats per inch.



(c)



(d)



(e)

Figure 5.2 (Continued)

5.3 Media Velocity Investigation

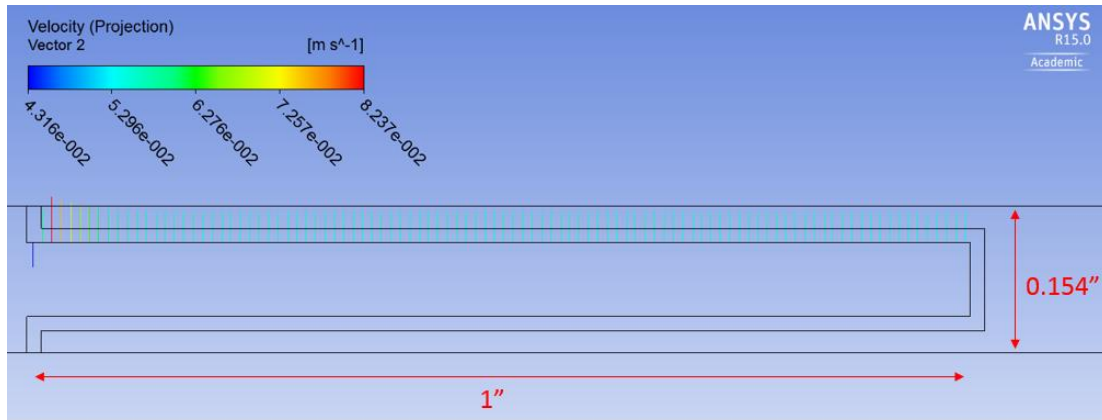
Unlike previous studies, which have investigated pleat count optimization for initial pressure drop across a clean unused filter element, the main performance objective of the current work is aimed at investigating the filtration velocity of various pleat configurations. To this end, the computational fluid simulation was manipulated to allow for the investigation of said parameter.

5.3.1 Media Velocity Profiles

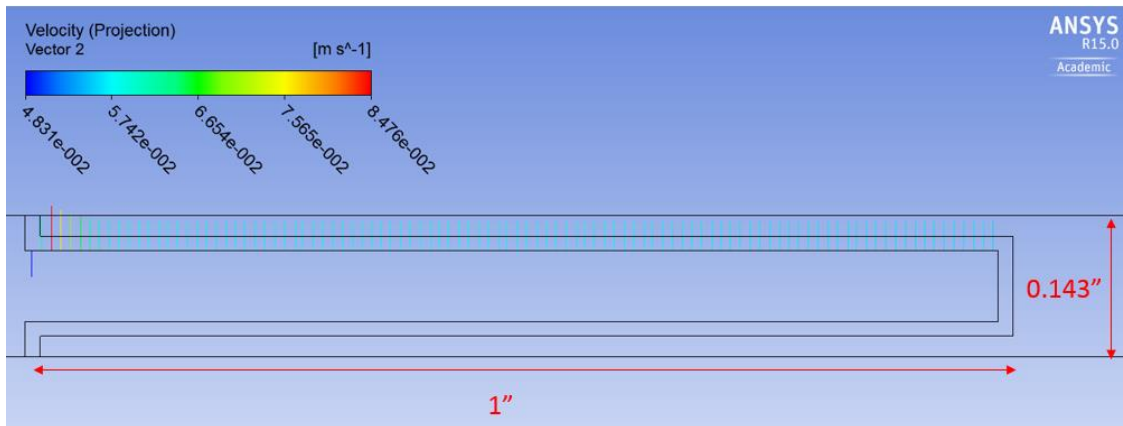
Using the built in CFD post processing functionality, included in ANSYS Workbench, the simulation was interrogated to determine the maximum value of the velocity component normal to the filtration surface along the length of the pleat. To accomplish this, the line representing the top side of the upstream media/fluid interface was prescribed as a “named selection” in ANSYS Workbench set-up tool. This allowed the line to be selected in the post processing tool and a vector plot to be defined along that line. The plot was chosen to display the velocity normal to the line as this would correspond to filtration media velocity.

The original hypothesis theorized that the shape along the pleat would be parabolic with a local maximum at the middle of the pleat and decreasing in magnitude from there to the root and tip of the pleat. The results however, show a curve with a maximum at the upstream tip of the pleat which quickly reduces and becomes somewhat uniform along the length of the pleat down to the root. It is posited that the local maximum evidenced in the simulation is due to the change in momentum the flow experiences upon contraction into the pleat. As the flow from the edges of the pleat channel turns to enter into the middle of the pleat a “y” component of velocity is introduced and the momentum associated with this “y” component is what causes the local

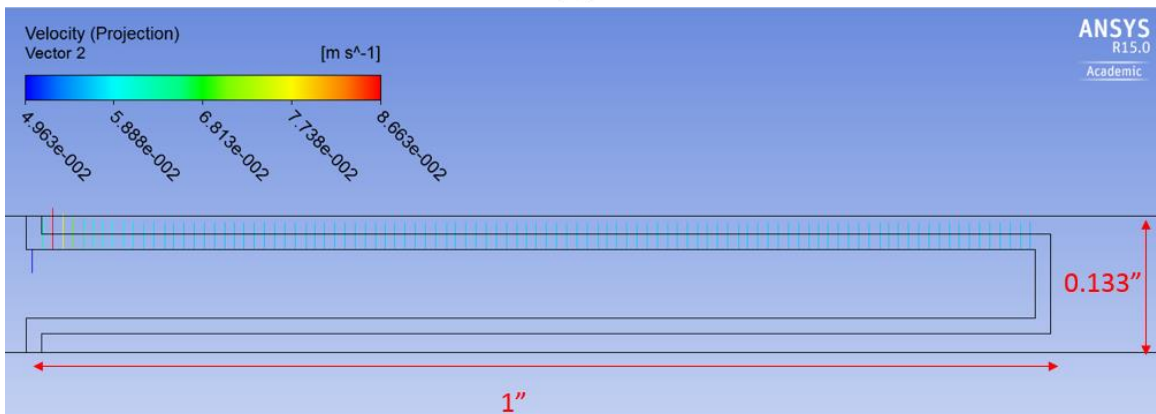
filtration velocity maximum. Figures 5.3a through 5.3e below provide an overview of the filtration velocity distributions for a representative sample of the individual cases studied.



(a)

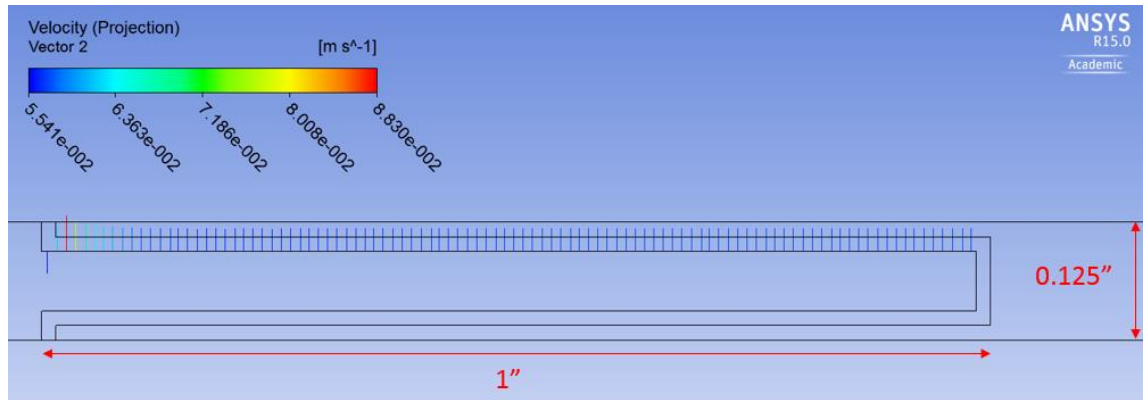


(b)

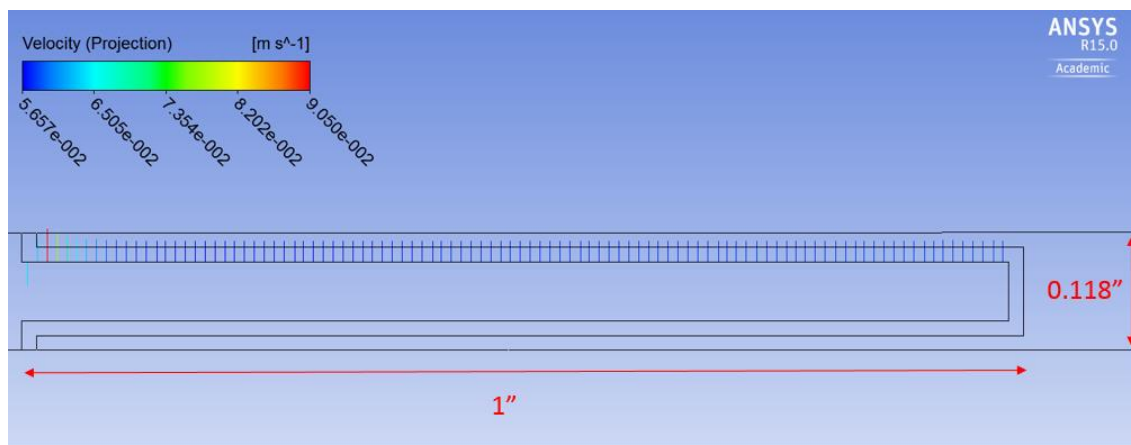


(c)

Figure 5.3 Media velocity profiles for various cases. Each case having a 10.5 ft/min assumed uniform media velocity with pleat configurations 1 inch in pleat height and (a) 6.5 pleats per inch (b) 7.0 pleats per inch (c) 7.5 pleats per inch (d) 8.0 pleats per inch and (d) 8.5 pleats per inch.



(d)



(e)

Figure 5.3 (Continued)

5.3.2 Media Velocity Maximum Values

The probe tool, built into the ANSYS Workbench application CFD Post, was employed to determine the maximum local values for the media velocity in each configuration. The tool was set up to probe only the v component of velocity. Figure 5.4 below shows an example of the probe being used and the value returned. The grey box in the image provide the user with feedback so one knows which area is being probed.

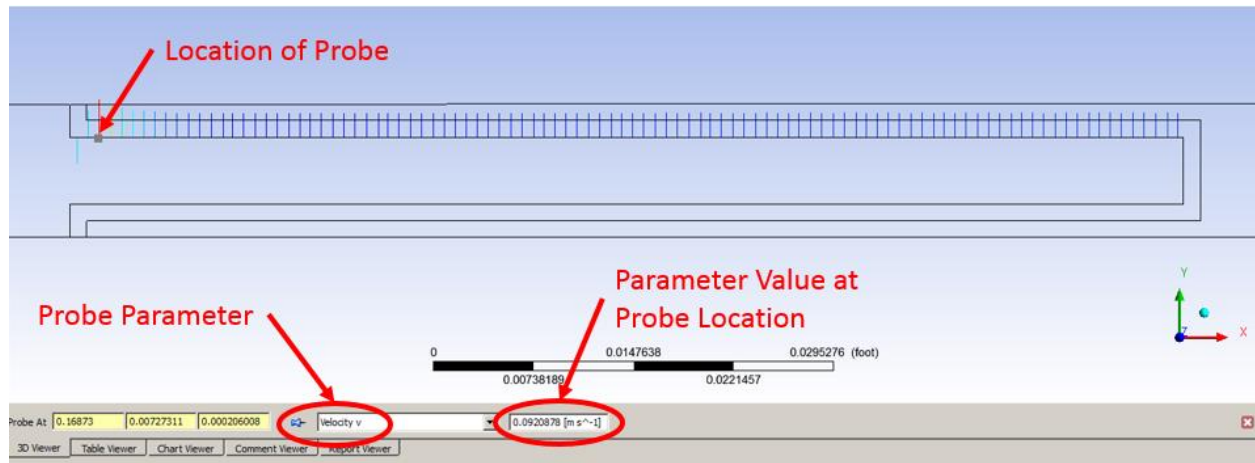


Figure 5.4 Example of probe tool being used to evaluate local filtration velocity.

The tool was used to probe a variety of points along the filter interface around the indicated local maximum to determine the maximum filtration velocity. For each case the parameter value, reported in meters per second, was rounded to the nearest thousandth and recorded. This value was converted to the equivalent velocity in units of feet per minute. Table 5-1 above lists the maximum filtration velocity for each case.

5.4 Relationship between Various Study Parameters

After simulation of the experimental domain, the maximum velocities were cataloged and several comparisons were made. It was hypothesized that there would be a direct relationship between the geometric aspect ratio and the ratio of maximum to average media velocity. Initial attempts investigated the dimensionless parameters aspect ratio and normalized maximum velocity. These were determined not to be a viable path forward and the relationship was instead modeled by plotting the maximum velocity for various pleat configurations as a function of the average velocity. The last attempt yielded a linear relationship and was used to develop a more robust model.

5.4.1 Dimensionless Comparisons

The first attempts at rationalizing the dataset were based upon the thought that a single dimensionless relationship would exist between the aspect ratio of the pleat and the maximum simulated filtration velocity normalized to the average filtration velocity. It was hypothesized that this would yield a relationship capable predicting the max velocity for any pleat with only knowing the average velocity. The following figures outline the investigation. Figure 5.5 shows a plot of the aspect ratio along the abscissa and the ratio of maximum simulation velocity to average velocity along the ordinate. The simple relationship between V_{\max} and V_{avg} was identified after a consideration of the viscous term in the modified Darcy-Lapwood-Brinkman equation discussed in Chapter 4. Figure 5.6 is similar however the maximum simulation velocity is now squared and normalized to the square of the average velocity; this was done in an attempt to account for the friction effects of the flow through the system as the effects of friction are a function of the square of velocity.

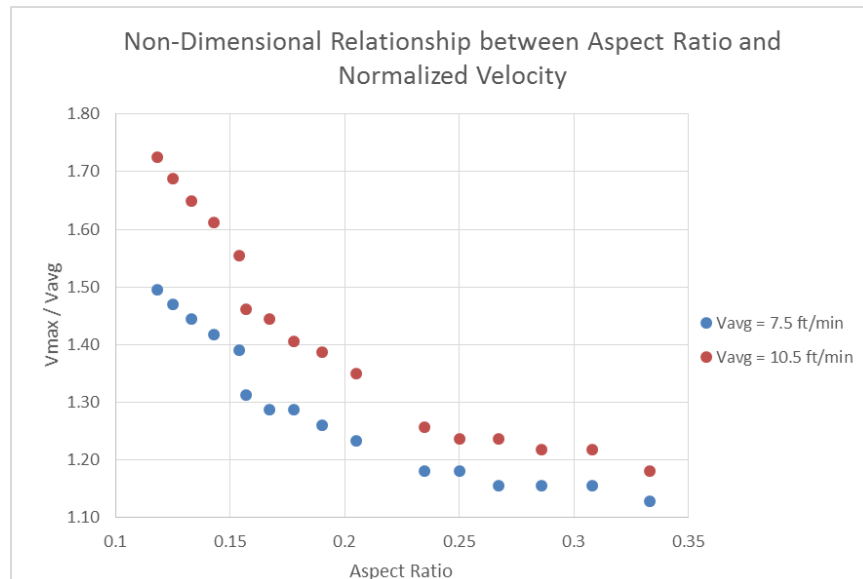


Figure 5.5 Plot of V_{\max}/V_{avg} vs. aspect ratio.

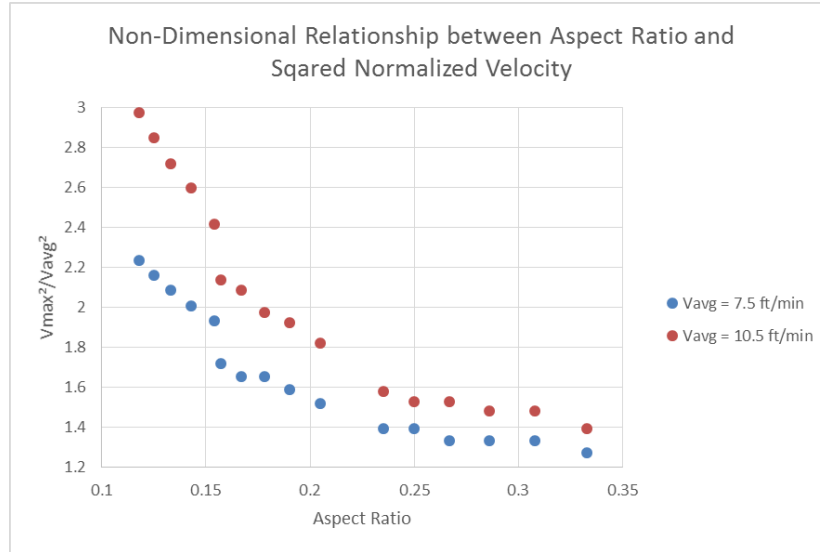


Figure 5.6 Plot of V_{max}^2/V_{avg}^2 vs. aspect ratio.

Examination of the plots above leads to two distinct conclusions. One, there does in fact appear to be a relationship between aspect ratio and the normalized maximum velocity. Two, this relationship is clearly not independent of the average velocity, as was previously hypothesized. It should also be noted that the steps, or groupings, in the above plots represent the different pleat heights that were employed to achieve the various aspect ratios in the current study. While the plots do show a relationship, it was determined that further investigation would not yield a simple model valid for multiple flow rates and pleat configurations.

To further investigate the relationship between the maximum filtration velocity and the average velocity from the uniform flow assumption, a plot was made to show the magnitude of maximum filtration velocity vs. average filtration velocity for various pleat configurations. This can be found in Figure 5.7 below. This is significant in that it shows a linear relationship between average and maximum velocity for each pleat configuration. This forms the basis of a promising tool developed in Section 5.5.3.

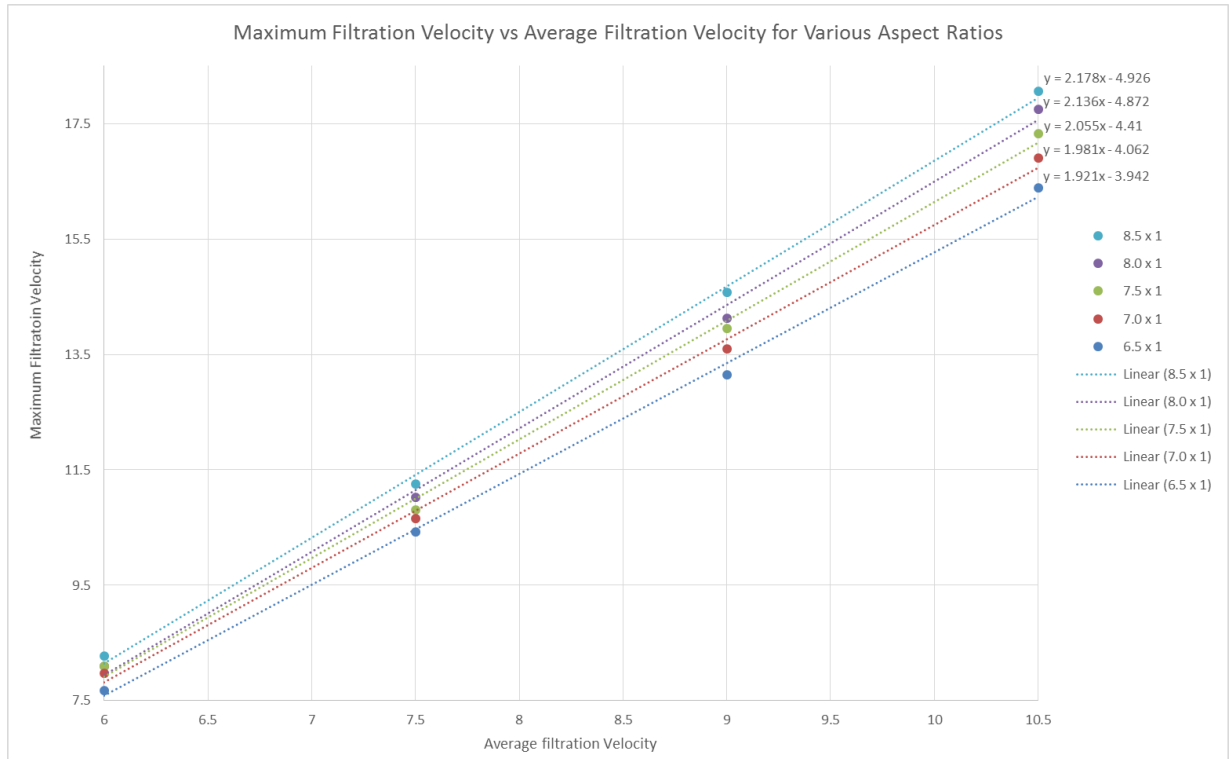


Figure 5.7 Plot of V_{max} vs. V_{avg} for various pleat configurations.

5.5 Evaluation of Maximum Media Velocities

Before proceeding further, it is beneficial to present an evaluation of the maximum simulation velocity in juxtaposition with the average velocity considered in the uniform flow assumption. From Table 5.1 it is clear that the maximum simulated filtration velocity exceeds the uniform flow assumption in every instance. It will be helpful to quantify the error associated with the uniform flow assumption. To this end, we will characterize the Absolute Relative Percent Error by the following equation:

$$\% \text{ Error} = \text{Abs} \left| \frac{\text{Average Velocity} - \text{Simulated Velocity}}{\text{Simulated Velocity}} \times 100 \right| \quad (15)$$

From Equation 15 above we can then evaluate the average and standard deviation of the error presented in the uniform flow assumption. The average absolute relative percent error is found to be 26.64% with a standard deviation of 8.02%. This will serve as the baseline for future

predictive models. Table 5.2 below is a heat map of the absolute relative error for the uniform flow assumption over the simulation domain.

Table 5.2 Absolute Relative Percent Error, Uniform Flow Assumption

Abs Relative % Error - Uniform Flow Assumption						
Legend		0.00	5.00	10.00	15.00	20.00
Pleat Density	Pleat Height	Face Velocity				
		10.5	9	7.5	6	
6.5 PPI	1.00	35.70	31.70	28.10	21.90	
	0.75	25.90		18.90		
	0.50	17.90		13.40		
7 PPI	1.00	37.90	33.70	29.40	23.80	
	0.75	27.90		20.60		
	0.50	17.90		13.40		
7.5 PPI	1.00	39.40	35.60	30.70	25.70	
	0.75	28.90		22.30		
	0.50	19.20		13.40		
8 PPI	1.00	40.70	35.60	30.70	25.70	
	0.75	30.70		22.30		
	0.50	19.20		15.30		
8.5 PPI	1.00	42.00	38.20	33.20	27.40	
	0.75	31.60		23.80		
	0.50	20.40		15.30		

5.5.1 Predictive Tools for Maximum Media Velocity

Two approaches were evaluated in the current work, the first sought to identify a single correction factor that could be applied to any average velocity that would yield a reasonable prediction of the maximum simulated filtration velocity for each configuration, the second attempted to leverage the linear relationship demonstrated in Figure 5.7. In both cases an evaluation of the prediction is carried out in the same manner as the evaluation of the uniform flow assumption in Section 5.5. This allows for a method to quickly quantify the suitability of each method. The tools laid forth in this paper are meant to aid the designer in the specification of filtration solutions to meet tight separation efficiency requirements where filtration velocity plays a large role in end item performance.

5.5.2 Correction Factor Tool

Correction factors are a common tool for the designer, from temperature knockdown factors, to stress concentration factors, fatigue limit factors and others. Designers and engineers are very familiar with the application of simple correction factors. It would therefore be beneficial to the designer to develop a tool that takes the form of the simple correction factor, as ease of use would most likely aid in adoption. The form of the tool for the designer would then take the form of the following equation:

$$V_{max} = \alpha \times V_{avg} \quad (16)$$

where α is the correction factor that relates the two velocity values.

To this end, an optimization problem was constructed and solved for using the solver tool in Microsoft Excel. First the variable α was initialized to a random value. Then a set of values was determined for V_{max} using equation X. The difference between the maximum simulated velocity and the max predicted velocity was the evaluated for each condition. The value for alpha was then iterated upon, using the aforementioned solver command, to force the sum of the differences between the predicted maximum velocity and the maximum simulated velocities to be zero. At the end of this routine the correction factor was 1.391. The average absolute relative error of this approach was found to be 9.56%. The single correction factor was then improved by running a second optimization routine to minimize the average absolute relative error. At the end of this routine the average absolute relative error was found to be 9.20% with a standard deviation of 5.71. The correction factor, α , was found to be 1.345. Table 5.3, below, provides a heat map displaying the values of absolute relative percent error across the study domain. This approach gives the designer a very simple tool and reduces the error in the uniform velocity assumption.

Table 5.3 Absolute Relative Percent Error, Correction Factor Tool

Abs Relative % Error - Correction Factor Tool					
Legend	0.00	5.00	10.00	15.00	20.00
Pleat Density	Pleat Height	Face Velocity			
		10.5	9	7.5	6
6.5 PPI	1.00	13.52	8.16	3.28	5.08
	0.75	0.34		9.05	
	0.50	10.42		16.48	
7 PPI	1.00	16.53	10.86	5.10	2.54
	0.75	3.07		6.75	
	0.50	10.42		16.48	
7.5 PPI	1.00	18.46	13.35	6.86	0.00
	0.75	4.32		4.53	
	0.50	8.72		16.48	
8 PPI	1.00	20.30	13.35	6.86	0.00
	0.75	6.84		4.56	
	0.50	8.72		13.85	
8.5 PPI	1.00	22.02	16.92	10.09	2.42
	0.75	8.00		2.52	
	0.50	7.07		13.85	

5.5.3 Linear Fitting Tool

As discussed previously, in section 5.4.1, a linear relationship exists between the maximum filtration velocity and the average filtration velocity of each pleat configuration. Therefore it is posited that a tool taking the y intercept form could be specified as follows:

$$V_{max} = m \times V_{avg} + b \quad (17)$$

where m and b are functions of the aspect ratio for the particular pleat design.

A platform was once again built in Microsoft Excel to aid in the investigation of possible values for m and b as a function of aspect ratio (denoted as “ar” in the following figures). Table 5.4 below shows the data that was used to drive the plots in Figure 5.7, shown in grey, as well as the evaluation of various fitting functions attempting to describe the slope of the line as a function of aspect ratio. Table 5.5 shows the same general approach to characterizing the y-intercept of Equation 17 as a function of aspect ratio.

Table 5.4 Investigation of Slope Fitting Parameter, Linear Fitting Tool

Config	6.5 x 1	7.0 x 1	7.5 x 1	8.0 x 1	8.5 x 1		
AR	0.154	0.143	0.133	0.125	0.118		
10.5	16.38	16.905	17.325	17.745	18.06		
9	13.14	13.59	13.95	14.13	14.58		
7.5	10.425	10.65	10.8	11.025	11.25		
6	7.68	7.98	8.1	8.1	8.28		
slope (m)	1.921	1.981	2.055	2.136	2.178	Function Avg	Std Dev
m/ar	12.47402597	13.85315	15.45113	17.088	18.45763		
m ^(1/ar)	69.35643867	119.1558	224.8892	433.3212	732.6512	315.875	242.9997
ar/m	0.08016658	0.072186	0.06472	0.058521	0.054178	0.066	0.009341
ar ^(1/m)	0.378	0.375	0.375	0.378	0.375	0.376	0.001453

Table 5.5 Investigation of Y-Intercept Fitting Parameter, Linear Fitting Tool

Config	6.5 x 1	7.0 x 1	7.5 x 1	8.0 x 1	8.5 x 1		
AR	0.154	0.143	0.133	0.125	0.118		
10.5	16.38	16.905	17.325	17.745	18.06		
9	13.14	13.59	13.95	14.13	14.58		
7.5	10.425	10.65	10.8	11.025	11.25		
6	7.68	7.98	8.1	8.1	8.28		
intercept (b)	-3.942	-4.062	-4.41	-4.872	-4.926	Function Avg	Std Dev
b/ar	-25.5974	-28.4056	-33.1579	-38.976	-41.7458		
-b ^(1/ar)	7383.967	18068.52	70049.16	317437.5	738918.7	230371.575	278100.7
ar/b	-0.03907	-0.0352	-0.03016	-0.02566	-0.02395	-0.031	0.005683
ar ^(1/b)	1.607342	1.614146	1.580058	1.532369	1.543164	1.575	0.032967
-b ^{ar}	1.235209	1.22194	1.218177	1.218887	1.20702	1.220	0.009031
ar ^b	1595.12	2697.895	7308.265	25110.45	37317.22	14805.788	14073.28

There were no direct criteria established for down selection of the defining functions but after consideration of several possible definitions the following equations defining the slope and y intercept, respectively, as functions of aspect ratio were chosen for further investigation:

$$0.376 = ar^{1/m} \quad (18)$$

$$1.220 = -b^{ar} \quad (19)$$

where ar is the aspect ratio, m is the slope, and b is the y intercept from Equation 17 above.

Rearranging Equations 18 and 19 from above and inserting them into Equation 17 yields:

$$V_{max} = \frac{\text{Log}(ar)}{\text{Log}(0.3176)} \times V_{avg} - 1.220ar^{\frac{1}{2}} \quad (20)$$

The tool was evaluated in the same manner as the average velocity and the correction factor tool. The average absolute relative percent error was found to be 4.19%, with a standard deviation of 4.02%. Table 5.6 below provides a heat map of the absolute relative error for the linear fitting tool.

Table 5.6 Absolute Relative Percent Error, Linear Fitting Tool

Abs Relative % Error - Linear Fitting Tool						
Legend		0.00	5.00	10.00	15.00	20.00
Pleat Density	Pleat Height	Face Velocity				
		10.5	9	7.5	6	
6.5 PPI	1.00	0.74	3.04	2.68	2.08	
	0.75	1.40		2.81		
	0.50	16.00		17.68		
7 PPI	1.00	0.32	2.22	2.52	0.55	
	0.75	2.67		4.49		
	0.50	10.54		12.24		
7.5 PPI	1.00	0.78	0.90	1.62	1.91	
	0.75	4.88		5.52		
	0.50	7.00		7.31		
8 PPI	1.00	1.73	0.39	0.06	2.76	
	0.75	5.12		8.20		
	0.50	2.50		5.03		
8.5 PPI	1.00	3.08	2.06	2.07	6.82	
	0.75	6.39		8.24		
	0.50	0.10		1.06		

CHAPTER 6: CONCLUSIONS AND FUTURE WORK

6.1 Conclusions

The performance of pleated air filters is investigated in this thesis. Unlike previous studies which address issues related to pleat count optimization for clean pressure drop, the current thesis is concerned with the prediction of the maximum filter velocity, as this parameter is directly tied to separation efficiency performance. It has been noted that a common practice in industry is to evaluate the average filter velocity as a means to predict separation efficiency performance. This can lead to errors in design, which results in products having to go through expensive and time consuming redesign processes to achieve the desired level of filtration performance. Additionally, there are some filters that are designed in a conservative manner to avoid this pitfall. Instead of being subject to a non-recurring onetime cost of redesign, these filters are over designed for the end application and while they pass initial qualification efforts, a substantial amount of wasted material and labor goes into each filter. In this case, the poor filter design leads to excess waste and recurring cost. It was concluded based off of industry experience that a better prediction tool would be needed. To this end, a commercially available computational fluid dynamics solver was employed to develop a robust simulation model of air flow through a pleated glass fiber filtration media. The model was employed over a range of pleat geometries and flow rates to simulate the flow field in and around the filtration media based on previous work. It was hypothesized that the filtration velocity at the pleated filter interface was not distributed evenly, and thus deviated from the assumption of uniform flow with an average filtration velocity. The simulations bore out that the magnitude of the filtration velocity

is in fact non-uniform along the length of the pleat. Two tools were presented to allow the filter designer to better predict maximum filtration velocity, a parameter directly linked to separation efficiency performance.

Unlike the previous simulation studies, the simulation in this thesis was developed in such a manner that the normal component of velocity at the filtration interface could easily be interrogated. The results of the simulations showed that there is indeed a local maximum for the filtration velocity. The local maximum velocity was observed at the tip of the upstream pleat form. A clear relationship was observed between the magnitude of deviation of the maximum velocity from the average velocity and the geometry of the pleat. It was found that as the pleat channel became narrower and the height of the pleat was increased, the amount of deviation increased. A non-dimensional term was introduced to quantify the steepness of the pleat, this term was referred to as the aspect ratio. Several non-dimensional plots were developed to further investigate the relationship between aspect ratio, average media velocity, and the maximum simulated media velocity. Based on the maximum simulated filtration velocities, the average absolute relative percent error for the uniform flow condition was shown to be 27%.

As part of the current thesis, two tools were developed and evaluated to help the designer better predict the maximum filtration velocity. The first tool was in the form of a simple knockdown correction factor. The tool predicts the maximum velocity as a linear function of the average velocity with no offset. The correction factor approach was evaluated for absolute relative percent error. This tool produced predicted maximum velocities with an average error on the order of 10%, a greater than two-fold reduction in error from the uniform flow assumption. Additionally, a linear fitting tool was developed based off the plotted results. This tool defined a standard relationship in the form of the slope intercept equation that predicted the maximum

velocity as a function of the average velocity and the aspect ratio of the pleat geometry. In this equation, the slope and y-intercept were defined as functions of aspect ratio. This approach predicted the maximum filtration velocity with an average absolute relative error of 4%, a greater than six-fold reduction in error from the uniform flow assumption.

6.2 Future Work

While every effort was made to build a simulation with high levels of fidelity, including an extensive validation against flat sheet filter media empirical data, the results presented herein come strictly from simulation. A clear area of opportunity to refine this work in the future exists in the form of the development of an empirical based study which seeks to define the maximum filtration velocity using experimental data. Not only would such work produce a dataset with a higher level of confidence, these results could then be fed back into the model development and a more robust model could be used in future simulations.

Additional future work could seek to further define the effects of localized maximum velocity on overall separation efficiency. This work could be performed as a numerical exercise to begin with, which would then be further validated by experimentation. Any models derived from such work could be used directly with the tools developed herein to allow the designer to more accurately predict the fundamental performance parameter of separation efficiency.

Another possible avenue would be to perform a weighted average calculation of the flow through the porous medium and evaluate the efficiency based on the supplier supplied data for efficiency vs. flow rate.

LIST OF REFERENCES

- [1] R. C. Brown, *Air filtration : an integrated approach to the theory and applications of fibrous filters*. Oxford ; New York : Pergamon Press, 1993.
- [2] N. Bojdo and A. Filippone, "Performance prediction of inlet barrier filter systems for rotorcraft engines," *Journal of Aircraft*, Author abstract no. 6, p. 1903, 2011.
- [3] M. Rebaï, M. Prat, M. Meireles, P. Schmitz, and R. Baclet, "A semi-analytical model for gas flow in pleated filters," *Chemical Engineering Science*, vol. 65, no. 9, pp. 2835-2846, 5/1/ 2010.
- [4] D.-R. Chen, D. Y. H. Pui, and B. Y. H. Liu, "Optimization of Pleated Filter Designs Using a Finite-Element Numerical Model," *Aerosol Science and Technology*, vol. 23, no. 4, pp. 579-590, 1995/01/01 1995.
- [5] C. M. Tsang, "Analysis of Pleated Air Filters Using Computational Fluid Dynamics," Master of Applied Science, Graduate Department of Mechanical and Industrial Engineering, University of Toronto, National Library of Canada, 1997.
- [6] M. Rebai, M. Prat, M. Meireles, P. Schmitz, and R. Baclet, "Clogging modeling in pleated filters for gas filtration," *Chemical Engineering Research and Design*, vol. 88, no. 4, pp. 476-486.
- [7] S. Fotovati, S. A. Hosseini, H. Vahedi Tafreshi, and B. Pourdeyhimi, "Modeling instantaneous pressure drop of pleated thin filter media during dust loading," *Chemical engineering science*, Article no. 18, 2011.
- [8] F. M. White, *Viscous fluid flow* (McGraw-Hill series in mechanical engineering). New York, NY : McGraw-Hill Higher Education, ©2006.
- [9] W. C. Hinds, *Aerosol technology : properties, behavior, and measurement of airborne particles*. New York : Wiley, c1999.
- [10] "Indoor Air Quality Handbook," Industry Publication, 2013.
- [11] R. a. A. C. E. American Society of Heating, *ANSI/ASHRAE standard 55-2013 : Thermal environmental conditions for human occupancy*. Atlanta: ASHRAE, 2013.
- [12] R. a. A.-C. E. American Society of Heating and I. American National Standards, *Ventilation for acceptable indoor air quality*. 2016.
- [13] R. a. A.-C. E. American Society of Heating and I. American National Standards, *An American national standard gravimetric and dust-spot procedures for testing air-cleaning devices used in general ventilation for removing particulate matter*. Atlanta, GA: American Society of Heating, Refrigerating and Air-Conditioning Engineers, Inc., 1992.
- [14] R. a. A.-C. E. American Society of Heating and I. American National Standards, *Method of testing general ventilation air-cleaning devices for removal efficiency by particle size*. 2015.
- [15] (2017, 1/21/2017). *About K&N Engineering*. Available: <http://www.knfilters.com/knhistory.htm>

- [16] C. E. Smeltzer, M. E. Gulden, S. S. McElmury, W. A. Compton, and C. A. Solar Turbines International San Diego, *Mechanisms of Sand and Dust Erosion in Gas Turbine Engines*. Ft. Belvoir: Defense Technical Information Center, 1970.
- [17] H. Geng, *Semiconductor Manufacturing Handbook* (McGraw-Hill Handbooks). New York: McGraw-Hill Professional, 2005.
- [18] I. British Standards, "EN 1822: High efficiency particulate air filters (HEPA and ULPA)." (in English), 1998.
- [19] A. M. Saleh and H. Vahedi Tafreshi, "A simple semi-numerical model for designing pleated air filters under dust loading," *Separation and Purification Technology*, Article vol. 137, pp. 94-108, 11/24/24 November 2014 2014.
- [20] L. Svarovsky, *Solid-gas separation*. Amsterdam; New York: Elsevier Scientific Pub. Co., 1981.
- [21] C. N. Davies, *Air filtration*. London, New York, Academic Press, 1973., 1973.
- [22] N. M. Bojdo, "Rotorcraft Engine Air Particle Separation," 2012.
- [23] J. R. Hobbs, "Gas turbine engine air intake," ed: Google Patents, 1983.
- [24] H. T and N. J, "Particle separator with scroll scavenging means," ed: Google Patents, 1974.
- [25] A. Filippone and N. Bojdo, "Turboshaft engine air particle separation," *Progress in Aerospace Sciences*, Review Article vol. 46, pp. 224-245, 1/1/2010 2010.
- [26] N. Bojdo and A. Filippone, "Comparative study of helicopter engine particle separators," *Journal of Aircraft*, Author abstract
- [27] J. E. Lundquist and A. Thomas, "Inertial separator," ed: Google Patents, 2011.
- [28] K. Bull and P. Roux, "CABIN AIR FILTRATION SYSTEMS - Novel Technological solutions for Commercial Aircraft," in *40th International Conference on Environmental Systems*(International Conference on Environmental Systems (ICES): American Institute of Aeronautics and Astronautics, 2010.
- [29] O. World Meteorological, S. United, A. National Oceanic and Atmospheric, A. National Aeronautics and Space, P. United Nations Environment, and C. European, *Assessment for decision makers : scientific assessment of ozone depletion 2014*. 2015.
- [30] S. Kuwabara, "The Forces experienced by a Lattice of Elliptic Cylinders in a Uniform Flow at Small Reynolds Numbers," *Journal of the Physical Society of Japan*, vol. 14, no. 4, pp. 522-527, 1959.
- [31] N. Martys, D. P. Bentz, and E. J. Garboczi, "Computer simulation study of the effective viscosity in Brinkman's equation," *Physics of Fluids*, vol. 6, no. 4, pp. 1434-1439, 1994.
- [32] J. Bear, *Dynamics of fluids in porous media*. Courier Corporation, 2013.
- [33] H. H. S. Yu and C. H. Gduldung, "Optimized Ultra High Efficiency Filter for High-Efficiency Industrial Combustion Turbines," no. 78965, p. V004T11A002, 1992.
- [34] H. Theliander and M. Fathi-Najafi, "Simulation of the build-up of a filter cake," *Filtration & Separation*, vol. 33, no. 5, pp. 417-421, 1996/05/01 1996.
- [35] I. ANSYS, "ANSYS Meshing User's Guide," Software User's Guide, 2013.
- [36] I. ANSYS, "ANSYS FLUENT 12.0 User's Guide," 2009.
- [37] B. R. Munson, T. H. Okiishi, W. W. Huebsch, and A. P. Rothmayer, *Fundamentals of fluid mechanics*. Hoboken, NJ : John Wiley & Sons, Inc., [2013]

APPENDIX A: COMPLETE SIMULATION RESULTS

Comments

	10.5 ft/min	9 ft/min	7.5 ft/min	6 ft/min
Face Area	100 in ²	100 in ²	100 in ²	100 in ²
Slit Width	10 in ²	10 in ²	10 in ²	10 in ²
Length of Pack	10 in ²	10 in ²	10 in ²	10 in ²
Pleat Height	1 in ²	1 in ²	1 in ²	1 in ²
Mean Media Velocity (Vavg)	10.5 ft/min	9 ft/min	7.5 ft/min	6 ft/min
Media Thickness	0.015 in	0.015 in	0.015 in	0.015 in

	6.5 1/in	6.5 1/in	6.5 1/in	6.5 1/in
PPI	6.5 1/in	6.5 1/in	6.5 1/in	6.5 1/in
Pleat Height (L27)	1 in	1 in	1 in	1 in
Pleat Width (v33=v34)	0.154 in	0.154 in	0.154 in	0.154 in
Pleat Bottom (v29)	0.077	0.077	0.077	0.077
Pleat Tops (v25=v23)	0.038	0.038	0.038	0.038
Pleat Side (v26)	0.023	0.023	0.023	0.023
Aspect Ratio	0.154	0.154	0.154	0.154
Number of Pleats	65 #	65 #	65 #	65 #
Media Area	9.028 ft ²	9.028 ft ²	9.028 ft ²	9.028 ft ²
Volumetric Flow Rate	94.8 ACFM	81.3 ACFM	67.7 ACFM	54.2 ACFM
Face Velocity	136.5 ft/min	117 ft/min	97.5 ft/min	78 ft/min
Reynolds No (Pleat Channel)	177.807	152.4064	127.0053	101.6043
Max Simulation Velocity	16.33 ft/min	13.18 ft/min	10.43 ft/min	7.7 ft/min
Vmax/Vavg	1.55524	1.464	1.391	1.280
Max Predicted Velocity	16.45 ft/min	13.58 ft/min	10.71 ft/min	7.84 ft/min
Simulation % Relative Error	0.74 %	3.04 %	2.68 %	2.08 %
% Rel E (Uniform Assumption)	35.70 %	31.71 %	28.09 %	21.88 %

6.5 PPI - 0.75" - PH

PPI	6.5 1/in	6.5 1/in	6.5 1/in
Pleat Height (L27)	0.75 in	0.75 in	0.75 in
Pleat Width (v33=v34)	0.154 in	0.154 in	0.154 in
Pleat Bottom (v29)	0.077	0.077	0.077
Pleat Tops (v25=v23)	0.038	0.038	0.038
Pleat Side (v26)	0.023	0.023	0.023
Aspect Ratio	0.205	0.205	0.205
Number of Pleats	65 #	65 #	65 #
Media Area	6.771 ft ²	6.771 ft ²	6.771 ft ²
Volumetric Flow Rate	71.1 ACFM	50.8 ACFM	43.7 ACFM
Face Velocity	102.375 ft/min	73.125 ft/min	63.525 ft/min
Reynolds No (Pleat Channel)	133.356	95.25401	82.525
Max Simulation Velocity	14.17 ft/min	9.25 ft/min	7.233 ft/min
Vmax/Vavg	1.34952	1.233	1.155
Max Predicted Velocity	14.37 ft/min	9.51 ft/min	7.51 ft/min
% Relative Error	1.40 %	2.81 %	2.81 %
% Rel E (Uniform Assumption)	25.90 %	18.92 %	18.92 %

6.5 PPI - 1.0" - PH

PPI	6.5 1/in	6.5 1/in	6.5 1/in
Pleat Height (L27)	0.5 in	0.5 in	0.5 in
Pleat Width (v33=v34)	0.154 in	0.154 in	0.154 in
Pleat Bottom (v29)	0.077	0.077	0.077
Pleat Tops (v25=v23)	0.038	0.038	0.038
Pleat Side (v26)	0.023	0.023	0.023
Aspect Ratio	0.308	0.308	0.308
Number of Pleats	65 #	65 #	65 #
Media Area	4.514 ft ²	4.514 ft ²	4.514 ft ²
Volumetric Flow Rate	47.4 ACFM	33.9 ACFM	28.7 ACFM
Face Velocity	68.25 ft/min	48.75 ft/min	41.25 ft/min
Reynolds No (Pleat Channel)	88.9037	63.50267	54.0267
Max Simulation Velocity	12.79 ft/min	8.66 ft/min	7.233 ft/min
Vmax/Vavg	1.2181	1.155	1.155
Max Predicted Velocity	10.74 ft/min	7.13 ft/min	6.0267 ft/min
% Relative Error	16.00 %	17.68 %	17.68 %
% Rel E (Uniform Assumption)	17.90 %	13.39 %	13.39 %

7.0 PPI - 1" PH

PPI	7 1/in	7 1/in	7 1/in	7 1/in
Pleat Height (L27)	1 in	1 in	1 in	1 in
Pleat Width (v33=v34)	0.143 in	0.143 in	0.143 in	0.143 in
Pleat Bottom (v29)	0.071	0.071	0.071	0.071
Pleat Tops (v25=v23)	0.036	0.036	0.036	0.036
Pleat Side (v26)	0.021	0.021	0.021	0.021
Aspect Ratio	0.143	0.143	0.143	0.143
Number of Pleats	70 #	70 #	70 #	70 #
Media Area	9.722 ft ²	9.722 ft ²	9.722 ft ²	9.722 ft ²
Volumetric Flow Rate	102.1 ACFM	87.5 ACFM	72.9 ACFM	58.3 ACFM
Face Velocity	147 ft/min	126 ft/min	105 ft/min	84 ft/min
Reynolds No (Pleat Channel)	177.907	152.4064	127.0053	101.6043
Max Simulation Velocity	16.92 ft/min	13.58 ft/min	10.63 ft/min	7.87 ft/min
Vmax/Vavg	1.61143	1.50889	1.417333	1.311667
Max Predicted Velocity	16.87 ft/min	13.88 ft/min	10.90 ft/min	7.91 ft/min
% Relative Error	0.32 %	2.22 %	2.52 %	0.55 %
% Rel E (Uniform Assumption)	37.94 %	33.73 %	29.44 %	23.76 %

7.0 PPI - 1.25" PH

PPI	7 1/in	7 1/in	7 1/in
Pleat Height (L27)	0.75 in	0.75 in	0.75 in
Pleat Width (v33=v34)	0.143 in	0.143 in	0.143 in
Pleat Bottom (v29)	0.071	0.071	0.071
Pleat Tops (v25=v23)	0.036	0.036	0.036
Pleat Side (v26)	0.021	0.021	0.021
Aspect Ratio	0.190	0.190	0.190
Number of Pleats	70 #	70 #	70 #
Media Area	7.292 ft ²	7.292 ft ²	7.292 ft ²
Volumetric Flow Rate	76.5 ACFM	54.7 ACFM	45.7 ACFM
Face Velocity	110.25 ft/min	78.75 ft/min	65.25 ft/min
Reynolds No (Pleat Channel)	133.356	95.25401	82.525
Max Simulation Velocity	14.57 ft/min	9.45 ft/min	7.45 ft/min
Vmax/Vavg	1.38762	1.26	1.26
Max Predicted Velocity	14.96 ft/min	9.87 ft/min	7.87 ft/min
% Relative Error	2.67 %	4.49 %	4.49 %
% Rel E (Uniform Assumption)	27.93 %	20.63 %	20.63 %

7.0 PPI - 1.0" PH

PPI	7 1/in	7 1/in	7 1/in
Pleat Height (L27)	0.5 in	0.5 in	0.5 in
Pleat Width (v33=v34)	0.143 in	0.143 in	0.143 in
Pleat Bottom (v29)	0.071	0.071	0.071
Pleat Tops (v25=v23)	0.036	0.036	0.036
Pleat Side (v26)	0.021	0.021	0.021
Aspect Ratio	0.286	0.286	0.286
Number of Pleats	70 #	70 #	70 #
Media Area	4.861 ft ²	4.861 ft ²	4.861 ft ²
Volumetric Flow Rate	51.0 ACFM	36.5 ACFM	30.5 ACFM
Face Velocity	73.5 ft/min	52.5 ft/min	43.75 ft/min
Reynolds No (Pleat Channel)	88.9037	63.50267	54.0267
Max Simulation Velocity	12.79 ft/min	8.66 ft/min	7.233 ft/min
Vmax/Vavg	1.2181	1.154667	1.154667
Max Predicted Velocity	11.44 ft/min	7.60 ft/min	6.30267 ft/min
% Relative Error	10.54 %	12.24 %	12.24 %
% Rel E (Uniform Assumption)	17.90 %	13.39 %	13.39 %

Comments	10.5 ft/min	9 ft/min	7.5 ft/min	6 ft/min	
Comments	Face Area	100 in ²	100 in ²	100 in ²	
	Slit Width	10 in ²	10 in ²	10 in ²	
	Length of Pack	10 in ²	10 in ²	10 in ²	
	Pleat Height	1 in ²	1 in ²	1 in ²	
	Mean Media Velocity (Vavg)	10.5 ft/min	9 ft/min	7.5 ft/min	
Media Thickness	0.015 in	0.015 in	0.015 in	0.015 in	
2.5 PPI - 1" PH	PPI	7.5 1/in	7.5 1/in	7.5 1/in	7.5 1/in
	Pleat Height (L27)	1 in	1 in	1 in	1 in
	Pleat Width (v33=v34)	0.133 in	0.133 in	0.133 in	0.133 in
	Pleat Bottom (v29)	0.067	0.067	0.067	0.067
	Pleat Tops (v25=v23)	0.033	0.033	0.033	0.033
	Pleat Side (v26)	0.018	0.018	0.018	0.018
	Aspect Ratio	0.133	0.133	0.133	0.133
	Number of Pleats	75 #	75 #	75 #	75 #
	Media Area	10.417 ft ²	10.417 ft ²	10.417 ft ²	10.417 ft ²
	Volumetric Flow Rate	109.4 ACFM	93.8 ACFM	78.1 ACFM	62.5 ACFM
	Face Velocity	157.5 ft/min	135 ft/min	112.5 ft/min	90 ft/min
	Reynolds No (Pleat Channel)	177.807	152.4064	127.0053	101.6043
	Max Simulation Velocity	17.32 ft/min	13.97 ft/min	10.83 ft/min	8.07 ft/min
	Vmax/Vavg	1.64952	1.552222	1.444	1.345
	Max Predicted Velocity	17.19 ft/min	14.10 ft/min	11.01 ft/min	7.92 ft/min
% Relative Error	0.78 %	0.90 %	1.62 %	1.91 %	
% Rel E (Uniform Assumption)	39.38 %	35.58 %	30.75 %	25.65 %	
2.5 PPI - 1.25" PH	PPI	7.5 1/in	7.5 1/in	7.5 1/in	7.5 1/in
	Pleat Height (L27)	0.75 in	0.75 in	0.75 in	0.75 in
	Pleat Width (v33=v34)	0.133 in	0.133 in	0.133 in	0.133 in
	Pleat Bottom (v29)	0.067	0.067	0.067	0.067
	Pleat Tops (v25=v23)	0.033	0.033	0.033	0.033
	Pleat Side (v26)	0.018	0.018	0.018	0.018
	Aspect Ratio	0.178	0.133	0.133	0.133
	Number of Pleats	75 #	75 #	75 #	75 #
	Media Area	7.813 ft ²	7.813 ft ²	7.813 ft ²	7.813 ft ²
	Volumetric Flow Rate	82.0 ACFM	82.0 ACFM	58.6 ACFM	46.9 ACFM
	Face Velocity	118.125 ft/min	118.125 ft/min	84.375 ft/min	67.5 ft/min
	Reynolds No (Pleat Channel)	133.356	133.356	95.25401	75.75
	Max Simulation Velocity	14.76 ft/min	14.76 ft/min	9.65 ft/min	7.28 ft/min
	Vmax/Vavg	1.40571	1.40571	1.286667	1.286667
	Max Predicted Velocity	15.48 ft/min	15.48 ft/min	10.18 ft/min	7.52 ft/min
% Relative Error	4.88 %	4.88 %	5.52 %	5.52 %	
% Rel E (Uniform Assumption)	28.86 %	28.86 %	22.28 %	22.28 %	
2.5 PPI - 1.5" PH	PPI	7.5 1/in	7.5 1/in	7.5 1/in	7.5 1/in
	Pleat Height (L27)	0.5 in	0.5 in	0.5 in	0.5 in
	Pleat Width (v33=v34)	0.133 in	0.133 in	0.133 in	0.133 in
	Pleat Bottom (v29)	0.067	0.067	0.067	0.067
	Pleat Tops (v25=v23)	0.033	0.033	0.033	0.033
	Pleat Side (v26)	0.018	0.018	0.018	0.018
	Aspect Ratio	0.267	0.267	0.267	0.267
	Number of Pleats	75 #	75 #	75 #	75 #
	Media Area	5.208 ft ²	5.208 ft ²	5.208 ft ²	5.208 ft ²
	Volumetric Flow Rate	54.7 ACFM	54.7 ACFM	39.1 ACFM	30.5 ACFM
	Face Velocity	78.75 ft/min	78.75 ft/min	56.25 ft/min	45 ft/min
	Reynolds No (Pleat Channel)	88.9037	88.9037	63.50267	50.4167
	Max Simulation Velocity	12.99 ft/min	12.99 ft/min	8.66 ft/min	6.75 ft/min
	Vmax/Vavg	1.23714	1.23714	1.154667	1.154667
	Max Predicted Velocity	12.08 ft/min	12.08 ft/min	8.03 ft/min	6.15 ft/min
% Relative Error	7.00 %	7.00 %	7.31 %	7.31 %	
% Rel E (Uniform Assumption)	19.17 %	19.17 %	13.39 %	13.39 %	
8.0 PPI - 1" PH	PPI	8 1/in	8 1/in	8 1/in	8 1/in
	Pleat Height (L27)	1 in	1 in	1 in	1 in
	Pleat Width (v33=v34)	0.125 in	0.125 in	0.125 in	0.125 in
	Pleat Bottom (v29)	0.063	0.063	0.063	0.063
	Pleat Tops (v25=v23)	0.031	0.031	0.031	0.031
	Pleat Side (v26)	0.016	0.016	0.016	0.016
	Aspect Ratio	0.125	0.125	0.125	0.125
	Number of Pleats	80 #	80 #	80 #	80 #
	Media Area	11.111 ft ²	11.111 ft ²	11.111 ft ²	11.111 ft ²
	Volumetric Flow Rate	116.7 ACFM	100.0 ACFM	83.3 ACFM	66.7 ACFM
	Face Velocity	168 ft/min	144 ft/min	120 ft/min	96 ft/min
	Reynolds No (Pleat Channel)	177.807	152.4064	127.0053	101.6043
	Max Simulation Velocity	17.72 ft/min	14.17 ft/min	11.03 ft/min	8.07 ft/min
	Vmax/Vavg	1.68762	1.574444	1.470667	1.345
	Max Predicted Velocity	17.41 ft/min	14.23 ft/min	11.04 ft/min	7.85 ft/min
% Relative Error	1.73 %	0.39 %	0.06 %	2.76 %	
% Rel E (Uniform Assumption)	40.74 %	36.49 %	32.00 %	25.65 %	
8.0 PPI - 1.25" PH	PPI	8 1/in	8 1/in	8 1/in	8 1/in
	Pleat Height (L27)	0.75 in	0.75 in	0.75 in	0.75 in
	Pleat Width (v33=v34)	0.125 in	0.125 in	0.125 in	0.125 in
	Pleat Bottom (v29)	0.063	0.063	0.063	0.063
	Pleat Tops (v25=v23)	0.031	0.031	0.031	0.031
	Pleat Side (v26)	0.016	0.016	0.016	0.016
	Aspect Ratio	0.167	0.125	0.125	0.125
	Number of Pleats	80 #	80 #	80 #	80 #
	Media Area	8.333 ft ²	8.333 ft ²	8.333 ft ²	8.333 ft ²
	Volumetric Flow Rate	87.5 ACFM	87.5 ACFM	62.5 ACFM	50.0 ACFM
	Face Velocity	126 ft/min	126 ft/min	90 ft/min	72 ft/min
	Reynolds No (Pleat Channel)	133.356	133.356	95.25401	75.75
	Max Simulation Velocity	15.16 ft/min	15.16 ft/min	9.65 ft/min	7.28 ft/min
	Vmax/Vavg	1.44381	1.44381	1.286667	1.286667
	Max Predicted Velocity	15.94 ft/min	15.94 ft/min	10.44 ft/min	7.85 ft/min
% Relative Error	5.12 %	5.12 %	8.20 %	8.20 %	
% Rel E (Uniform Assumption)	30.74 %	30.74 %	22.28 %	22.28 %	
8.0 PPI - 1.5" PH	PPI	8 1/in	8 1/in	8 1/in	8 1/in
	Pleat Height (L27)	0.5 in	0.5 in	0.5 in	0.5 in
	Pleat Width (v33=v34)	0.125 in	0.125 in	0.125 in	0.125 in
	Pleat Bottom (v29)	0.063	0.063	0.063	0.063
	Pleat Tops (v25=v23)	0.031	0.031	0.031	0.031
	Pleat Side (v26)	0.016	0.016	0.016	0.016
	Aspect Ratio	0.250	0.250	0.250	0.250
	Number of Pleats	80 #	80 #	80 #	80 #
	Media Area	5.556 ft ²	5.556 ft ²	5.556 ft ²	5.556 ft ²
	Volumetric Flow Rate	58.3 ACFM	58.3 ACFM	41.7 ACFM	33.3 ACFM
	Face Velocity	84 ft/min	84 ft/min	60 ft/min	48 ft/min
	Reynolds No (Pleat Channel)	88.9037	88.9037	63.50267	50.4167
	Max Simulation Velocity	12.99 ft/min	12.99 ft/min	8.66 ft/min	6.75 ft/min
	Vmax/Vavg	1.23714	1.23714	1.181333	1.181333
	Max Predicted Velocity	12.67 ft/min	12.67 ft/min	8.41 ft/min	6.45 ft/min
% Relative Error	2.50 %	2.50 %	5.03 %	5.03 %	
% Rel E (Uniform Assumption)	19.17 %	19.17 %	15.35 %	15.35 %	

Comments	10.5 ft/min		9 ft/min		7.5 ft/min		6 ft/min		
	Value	Unit	Value	Unit	Value	Unit	Value	Unit	
8.5 PPI - 1" PH	Face Area	100	in ²	100	in ²	100	in ²	100	in ²
	Slit Width	10	in ²	10	in ²	10	in ²	10	in ²
	Length of Pack	10	in ²	10	in ²	10	in ²	10	in ²
	Pleat Height	1	in ²	1	in ²	1	in ²	1	in ²
	Mean Media Velocity (Vavg)	10.5	ft/min	9	ft/min	7.5	ft/min	6	ft/min
	Media Thickness	0.015	in	0.015	in	0.015	in	0.015	in
	PPI	8.5	1/in	8.5	1/in	8.5	1/in	8.5	1/in
	Pleat Height (L27)	1	in	1	in	1	in	1	in
	Pleat Width (v33~v34)	0.118	in	0.118	in	0.118	in	0.118	in
	Pleat Bottom (v29)	0.059		0.059		0.059		0.059	
	Pleat Tops (v25~v23)	0.029		0.029		0.029		0.029	
	Pleat Side (v26)	0.014		0.014		0.014		0.014	
	Aspect Ratio	0.118		0.118		0.118		0.118	
	Number of Pleats	85	#	85	#	85	#	85	#
	Media Area	11.806	ft ²	11.806	ft ²	11.806	ft ²	11.806	ft ²
Volumetric Flow Rate	124.0	ACFM	106.3	ACFM	88.5	ACFM	70.8	ACFM	
Face Velocity	178.5	ft/min	153	ft/min	127.5	ft/min	102	ft/min	
Reynolds No (Pleat Channel)	177.807		152.4064		127.0053		101.6043		
Max Simulation Velocity	18.11	ft/min	14.57	ft/min	11.22	ft/min	8.27	ft/min	
Vmax/Vavg	1.72476		1.618889		1.496		1.378333		
Max Predicted Velocity	17.55	ft/min	14.27	ft/min	10.99	ft/min	7.71	ft/min	
% Relative Error	3.08	%	2.06	%	2.07	%	6.82	%	
% Rel E (Uniform Assumption)	42.02	%	38.23	%	33.16	%	27.45	%	
8.5 PPI - 75" PH	PPI	8.5	1/in	8.5	1/in	8.5	1/in	8.5	1/in
	Pleat Height (L27)	0.75	in	0.75	in	0.75	in	0.75	in
	Pleat Width (v33~v34)	0.118	in	0.118	in	0.118	in	0.118	in
	Pleat Bottom (v29)	0.059		0.059		0.059		0.059	
	Pleat Tops (v25~v23)	0.029		0.029		0.029		0.029	
	Pleat Side (v26)	0.014		0.014		0.014		0.014	
	Aspect Ratio	0.157		0.157		0.157		0.157	
	Number of Pleats	85	#	85	#	85	#	85	#
	Media Area	8.854	ft ²	8.854	ft ²	8.854	ft ²	8.854	ft ²
	Volumetric Flow Rate	93.0	ACFM	93.0	ACFM	66.4	ACFM	66.4	ACFM
	Face Velocity	133.875	ft/min	133.875	ft/min	95.625	ft/min	95.625	ft/min
	Reynolds No (Pleat Channel)	133.356		133.356		95.25401		95.25401	
	Max Simulation Velocity	15.35	ft/min	15.35	ft/min	9.84	ft/min	9.84	ft/min
	Vmax/Vavg	1.4619		1.4619		1.312		1.312	
	Max Predicted Velocity	16.33	ft/min	16.33	ft/min	10.65	ft/min	10.65	ft/min
% Relative Error	6.39	%	6.39	%	8.24	%	8.24	%	
% Rel E (Uniform Assumption)	31.60	%	31.60	%	23.78	%	23.78	%	
8.5 PPI - 1/2" PH	PPI	8.5	1/in	8.5	1/in	8.5	1/in	8.5	1/in
	Pleat Height (L27)	0.5	in	0.5	in	0.5	in	0.5	in
	Pleat Width (v33~v34)	0.118	in	0.118	in	0.118	in	0.118	in
	Pleat Bottom (v29)	0.059		0.059		0.059		0.059	
	Pleat Tops (v25~v23)	0.029		0.029		0.029		0.029	
	Pleat Side (v26)	0.014		0.014		0.014		0.014	
	Aspect Ratio	0.235		0.235		0.235		0.235	
	Number of Pleats	85	#	85	#	85	#	85	#
	Media Area	5.903	ft ²	5.903	ft ²	5.903	ft ²	5.903	ft ²
	Volumetric Flow Rate	62.0	ACFM	62.0	ACFM	44.3	ACFM	44.3	ACFM
	Face Velocity	89.25	ft/min	89.25	ft/min	63.75	ft/min	63.75	ft/min
	Reynolds No (Pleat Channel)	88.937		88.937		63.50267		63.50267	
	Max Simulation Velocity	13.19	ft/min	13.19	ft/min	8.86	ft/min	8.86	ft/min
	Vmax/Vavg	1.25619		1.25619		1.181333		1.181333	
	Max Predicted Velocity	13.20	ft/min	13.20	ft/min	8.77	ft/min	8.77	ft/min
% Relative Error	0.10	%	0.10	%	1.06	%	1.06	%	
% Rel E (Uniform Assumption)	20.39	%	20.39	%	15.35	%	15.35	%	

APPENDIX B: LYDAIR 4450HS PRODUCT DATASHEET

4450-HS

TYPICAL PROPERTY SHEET



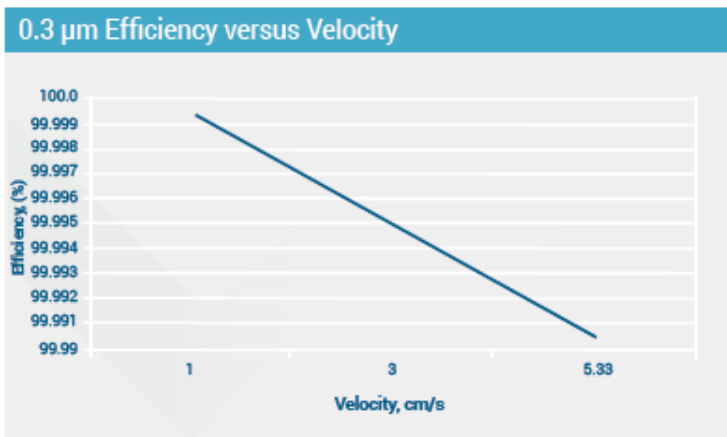
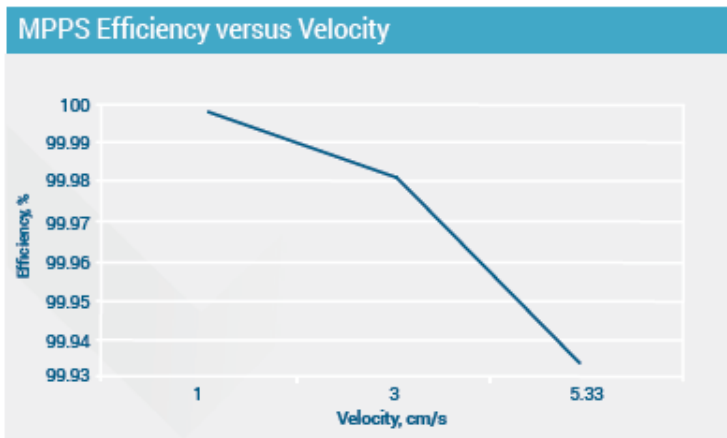
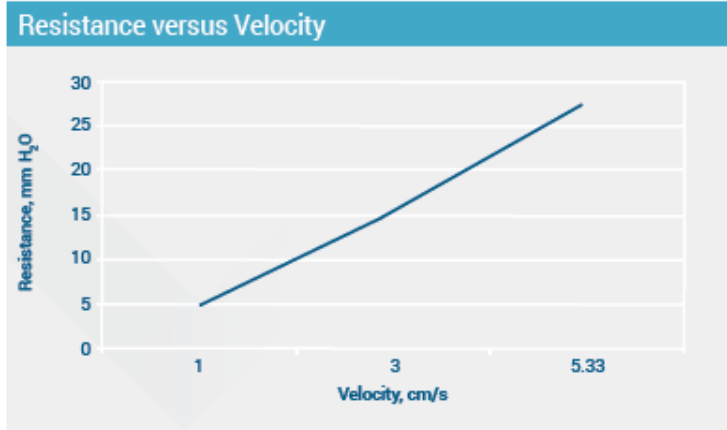
- Applications**
- Chemical Processing
 - Clean and Bio-Safety Benches
 - Cleans Rooms
 - Commercial/Industrial/Institutional HVAC
 - Micro and Mini Environments
 - Personal Respirators
 - Pharmaceutical Semiconductor Manufacturing
 - Room Air Purifiers

High Alpha HEPA Air Filtration

LydAir® MG High Alpha HEPA air filtration media are engineered for use in a wide range of absolute clean air applications. Specially engineered to provide the highest available efficiency at a minimal resistance to air flow, LydAir MG is chosen for applications where guaranteed efficiency and consistency is a must and reduced energy costs can provide a distinguishable competitive advantage.

- Custom-engineered to meet specific applications
- Available for:
 - Manual or fully automatic pleating operations
 - Deep or mini-pleat applications

4450-HS Typical Properties						
Typical Properties	US Customary		SI Units		Reference Test Methods	
Basis Weight	48	lbs/3000 ft ²	78	g/m ²	T.A.P.P.I. - T - 410 A.S.T.M. - D - 546	
Thickness (7.3psi / 50 kPa)	14.5	mils	0.37	mm	T.A.P.P.I. - T - 411	
Tensile	MD	3800	g/inch	37	N/inch	T.A.P.P.I. - T - 494
	CD	1400	g/inch	14	N/inch	T.A.P.P.I. - T - 494
Stiffness, MD	1200	mg	1200	mg	T.A.P.P.I. - T - 543	
LOI	6	%	6	%	T.A.P.P.I. - T - 413	
Penetration (0.3µm DEHS @ 5.33 cm/s)	0.018	%	0.018	%	MIL - STD - 282 A.S.T.M. - D2986-91	
Air Resistance (5.33 cm/s)	29	mm	284	Pa	MIL - STD - 282 A.S.T.M. - D2986-91	
Water Repellency	22	Inches	560	mm	MIL - STD - 282	



Note: All product data is nominal and does not represent a specification.

All data and statements concerning these products may be considered as being indicative of representative properties and characteristics obtainable. We make no warranty, expressed or implied, concerning actual use or results because of industry specific influences.



Lydall Performance Materials

www.lydallpm.com

info@lydall.com

North America & Asia: +1 603 332 4600

Europe, Middle East & Africa: +33 (0) 2 97 28 5300

Rev. Date: 02/04/2016


All rights reserved. Copyright 2016

APPENDIX C: COPYRIGHT PERMISSIONS

Below is permission for the use of material in Table 2.1

ASHRAE standard

Order detail ID: 70352654
Order License Id: 4071960809233
ISSN: 1041-2336
Publication Type: Monographic Series
Volume:
Issue:
Start page:
Publisher: THE SOCIETY,
Author/Editor: AMERICAN SOCIETY OF HEATING,
REFRIGERATING AND AIR

Permission Status:  **Granted**

Permission type: Republish or display content
Type of use: Republish in a thesis/dissertation

[View details](#)